Memòria final del màster de Física
Programa de Doctorat del Departament de Física

A hydro-meteorological modeling study of a flash-flood event over Catalonia, Spain

Arnau Amengual Pou
Grup de Meteorologia
Departament de Física
Universitat de les Illes Balears
Setembre, 2006

Al meu país la pluja no sap ploure:
o plou poc o plou massa;
si plou poc és la sequera,
si plou massa és la catàstrofe.
Qui portarà la pluja a escola?
Qui li dirà com s'ha de ploure?
Al meu país la pluja no sap ploure.

Raimon,
extracte del disc 'Entre la nota i el so'
(1984)

AGRAÏMENTS

Al Departament de Física de la Universitat de les Illes Balears com a estudiant de tercer cicle.

De forma més particular, a tots els components del Grup de Meteorologia y de manera més propera als co-autors d'aquest treball: en Romu, n'Alberto i en Sergio. També voldria agraïr a en Sergio i a en Romu, co-directors de la memòria, la confiança i comprensió mostrades des de que em vaig integrar al Grup.

No voldria oblidar-me d'un altre dels co-autors de l'estudi, el Dr. Manuel Gómez, de la Secció d'Enginyeria Hidràulica i Hidrològica del Departament d'Enginyeria Hidràulica, Marítima i Ambiental de la Universitat Politècnica de Catalunya. També recordar la inestimable ajuda i paciència mostrada per en Thomas A. Evans, Senior Hydraulic Engineer of the HEC-HMS Hydrologic Engineering Center (Davis, CA, USA).

Finalment, i d'una manera molt especial: a n'Anna, a la família i tots els amics pel seu continu recolçament.

CONTENTS

SUMMARY OF THE STUDY

During the early morning on 10 June 2000, the Catalonia region was affected by a hazardous convective rainfall episode which produced a large increase on flow regimes in many internal catchments of the region. The present modeling study is focussed upon the Llobregat basin, the biggest internal catchment with a drainage area of 5040 km^2. The first objective of the study is the characterization of the watershed hydrological response to this flash-flood event based on rain-gauge data and HEC-HMS runoff model. The HEC-HMS model has been calibrated using five episodes of similar torrential characteristics, and the effects of the spatial segmentation of the basin and of the temporal scale of the input rainfall field have been examined. These kind of episodes present short recurrence intervals in Mediterranean Spain and the use of mesoscale forecast driven runoff simulation systems for increasing the lead-times of the emergency management procedures is a valuable issue to explore. The second objective uses NCEP and ECMWF analyses to initialize the MM5 non-hydrostatic mesoscale model in order to simulate the 10 June 2000 flash-flood episode with appropriate space and time scales to force the runoff model. The final objective analyses the sensitivity of the catchment's response to the spatial and temporal uncertainty of the rainfall pattern based on an ensemble of perturbed MM5 simulations. MM5 perturbations are introduced through small shifts and changes in intensity of the precursor upper-level synoptic scale trough. Main results indicate that: **(1)** an optimum configuration of the runoff model can be clearly defined that best adjusts the simulated basin's hydrological response to observed peak discharges, their timing and total volume; **(2)** the MM5-control driven runoff simulation shows a reasonable reproduction of the observed discharge at the basin's outlet and appears to be a suitable tool for the hydro-meteorological forecasting of flash-floods in the Llobregat basin as a whole; **(3)** the ensemble of perturbed runoff simulations does not exhibit any relevant degradation of the forecast skill and some of the members even outperform the control experiment at different stream-gauges locations. That is, the catchment is relatively insensitive to rainfall forecast errors of a few tenths of kilometres and no more than 1-2 hours.

Chapter 1

INTRODUCTION

1.1 Flash-flood events in the Spanish Mediterranean area

The human life, society and property are essentially fragile elements, susceptible to hazardous episodes caused by the environment. Sometimes and more frequently in some areas than others, such hazardous episodes can be so great or can have a big impact in densely populated or developed areas producing important damages. These natural impacts can be of many several kinds and they can have special features in the different climatological and geomorphologic regions of the world. About the 60% of these disasters are related to hurricanes and to floods. Flooding events in low lands due to large rivers have return periods of many decades and flood-prone areas are quite easily identified. In addition, floods occur over periods of several days and it is possible to attemp damage mitigation. The situation can be quite different in the southern European region, and concretely along the Mediterranean coast line, where extreme flooding events are experienced in urban areas very frequently in time, but randomly in space, especially during the fall season. The flash-flood episodes are distinguised from the 'ordinary' floods by the time scale of the events: the worst of these can develop in periods of a few hours or less after the rainfall and their occurrence is too rapid to attempt damage mitigation. This makes flash-floods particularly dangerous in terms of human lifes and properties.

A flash-flood is a hydro-meteorological event that depends on both hydrological and meteorological factors. The meteorological factors play a basic role when rainfall becomes

intense and that intensity is maintained long enough to create the potential for flash-floods. The hydrological factors also plays a large role in these kind of episodes; a given amount of rainfall in a given period of time can or cannot result in a flash-flood owing to factors as: the antecedent precipitation and therefore the antecedent moisture condition of the soil, the soil permeability, the terrain slope, the land use or the vegetation cover. As consequence, flash-flood forecasting involves both a hydrological and a meteorological forecast (Doswell, 1994; see figs. 1.1 and 1.2 in order to notice the relation between the spatio-temporal scales of the atmospheric and the hydrologic processes).

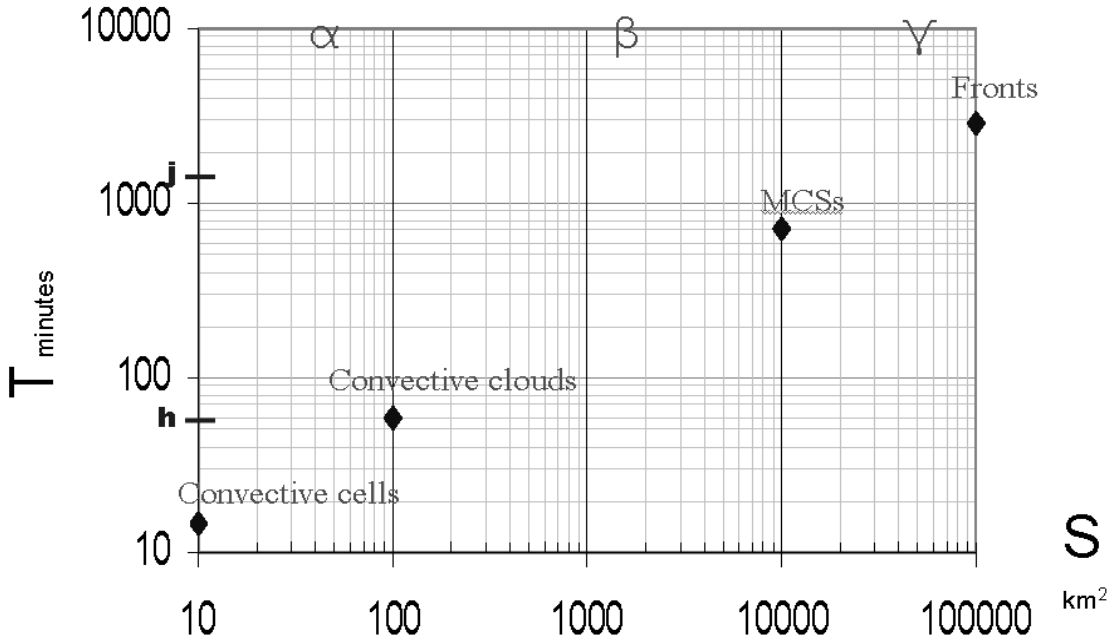

Figure 1.1: Scale subdivision for the atmospheric processes and their orders of magnitude (after Orlanski, 1975).

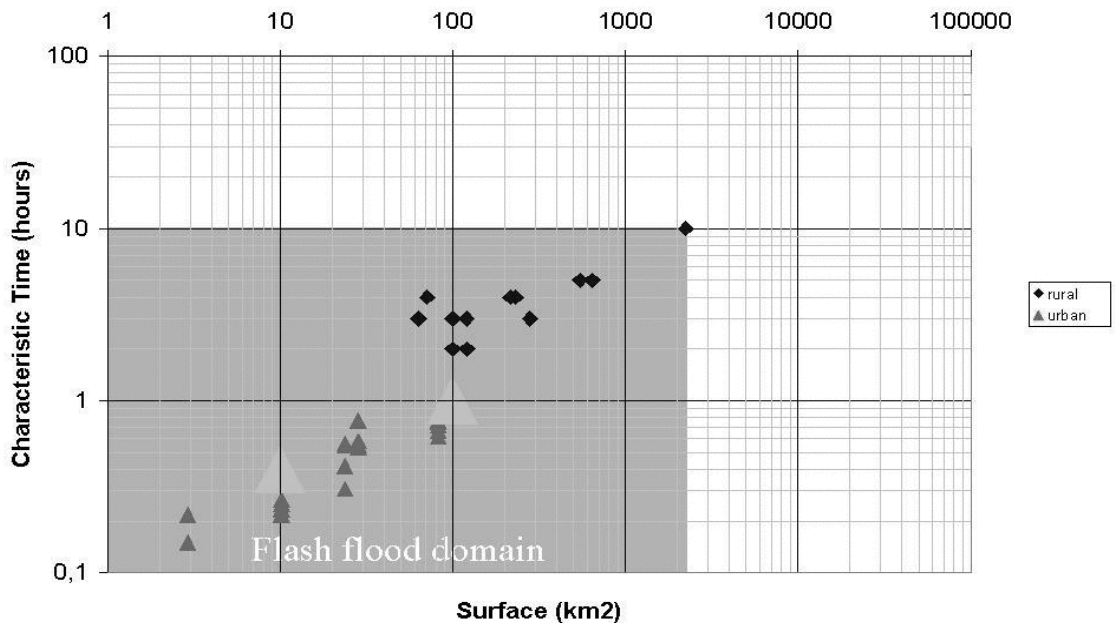

Figure 1.2: Flash-flood domain for rural and urban areas.

Below, the most relevant physical and social factors are briefly reviewed which together produce a high risk threshold in the Mediterranean area to flash-floods.

1. *The meteorological conditions*

   In the western Mediterranean area, as the summer eastward extension of the Azores high pressure cell moves back towards low latitudes and the pressure drop occurs in the early autumn, a marked increase in the probability of intense precipitation rates rises, certainly favoured by the high sea surface temperature of the Mediterranean Sea. These changes in the synoptic patterns are associated with the early invasion of cold fronts. As described in Doswell et al. (1996), flash-floods are the result of high precipitation rates persisting for a relatively long time (order of a few hours). The minimum amount of rainfall and its duration to create flash-flood conditions depends on the hydrological setting for the episode. It seems clear that the majority of flash-flood-producing rainfall is convective. This is because the rapid upward vertical motion in convection also promotes high precipitation rates. Since not all convective storms produce flash-floods, a major limiting effect is the duration of the

relatively intense convective rainfalls. Most convective events do not persist in any given catchment long enough to produce flooding, so the duration of convection is the key issue. In the flash-flood cases, the convection is maintained over a specific location as 'quasi-stationary convective events' (Chappell, 1986). What makes the convection remain geographically fixed for an extended period is the development of new convective cells, forming multi-clusters called mesoscale convective systems (MCSs), so as to nearly cancel the tendency of such cells to drift with the wind.

Heavy rainfalls can also result from the forced ascent of moist air in stable stratification. This is associated with orographically-forced rainfall events and in some cases quasi-stationary convection occurs in situations involving an orographic component where the convective element can develop because ascent tends to reduce the static stability, but convection is not the dominant contributor of rainfall (Romero et al. 1998). Then, into the Mediterranean region, extreme rainfalls often result from the thermal effects induced by relatively high sea surface temperatures in that season together with the incursion of cold air masses leading to convective instabilities along the cold fronts producing interactions between frontal and orographic enhancement (Ramis et al., 1994). The resulting space and time scales of heavy rainfall patterns are highly variable depending on the structure of the large scale circulation and on the local orographic features.

2. *The urban conditions*

As aforementioned, hydrology plays a major role in the occurence of flash-floods. Of particular significance to flash floods are: (i) the antecedent precipitation related directly with the moisture of the soil and its infiltration properties; (ii) the terrain, and (iii) the surface runoff characteristics. The last two issues are of crucial importance in the Mediterranean area since the space left for the rivers flowing through the historical cities, sometimes is enough to carry ordinary floods but not the disastrous ones. Furthermore, the high urbanization rate in coastal areas and the absence of a planning capability in all these places increase the risks involved

in these kind of events, most of them owing to the development of the building rate when the knowledge of the involved hydrological risks was rather poor (Siccardi, 1996). In fact, the streams and rivers along the Mediterranean coast are usually dry for most part of the year, but develop flash floods during storms with the associated hydrograph peaks in short periods of time (of some hours; see figs. 1.2 and 1.3 in order to notice the effect of urbanization on storm runoff).

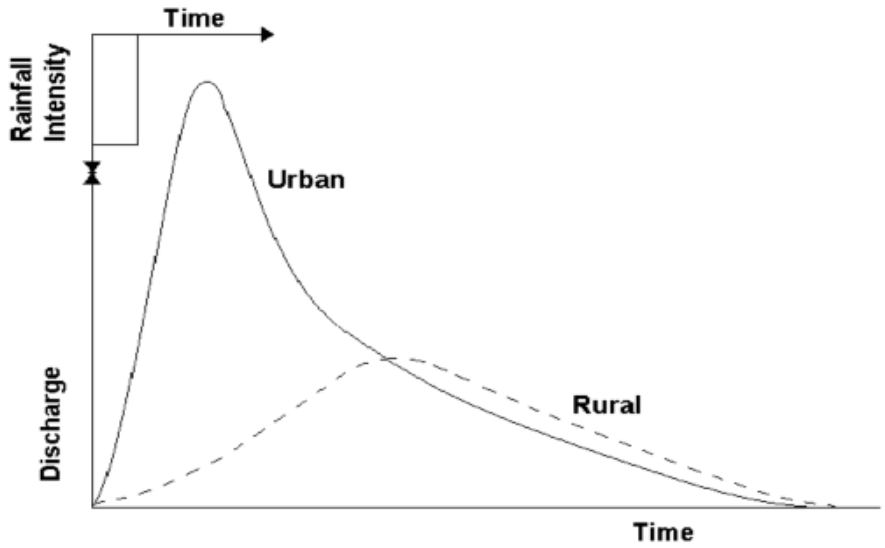

Figure 1.3: Flood hydrographs for urbanized and natural basins.

The sum of all these abovementioned factors can be summarized for the Spanish Mediterranean area as follows:

(i) Its topography makes it especially prone to flash flood events: mountain systems near the coast usually act as natural barriers to the warm moist mediterranean air, inducing the generation of intense rainfall rates that show high variability in space and time.

(ii) Serious damage can occur when intense convective rainfall events combine with short hydrological response times, characteristic of steep streams and increasing urbanization rates in coastal areas. Furthermore, in this semiarid environment many

small and medium steep streams are ephemeral, which can cause unexpected and extensive flood damage. Increased flows over short periods, high flow velocities and large volumes of sediment constitute threats to property and human life (Martín-Vide et al. 1999).

3. *Spatial and temporal scales of the meteorological predictions and their related uncertainties*

   Global circulation models of the atmosphere (GCMs), as they are operationally run by meteorological offices, can provide suitable weather predictions with a lead time up to 48-96 hours, and parameterize rainfall over spatial windows of the order of $\sim 10^4$ km^2, the size of the elementary grid for the numerical solution of the governing equations. The orography is accordingly resolved at the same space scale. As consequence, many of the watersheds of the Mediterranean coastline are lost for these coarse resolutions. In order to address these issues, the limited area models (LAMs) -nested inside the GCMs- provide a better space discretization and operational LAMs are run with space windows of tenths of km^2. The predictions of such weather patterns is then quite satisfactory resolved and this present status enables them to be used as a trigger for flood warning systems, targetting large regions as the Spanish Mediterranean coast and the Balearic Islands.

   Although LAMs can produce highly realistic mesoscale structures, however, the associate forecasts errors reduce the confidence in the model fields, especially for convective systems and precipitation. The sensitivity of small-scale features in the forecast to errors in the initial and boundary conditions databases or the approximations in the physical parameterizations which are included in the mesoscale models determine the degree of predictability of such episodes (Martín et al. 2006). Taking into account all these factors, it is very important to explore the possibility of obtaining as much as possible accurate forecasts of the rising flows before these kind of episodes and to assess the impact of the abovementioned external-scale uncertainties in the hydro-meteorological chain.

1.2 Scope of the study

During flooding events the amount of time available for the implementation of emergency management procedures is limited. It must be examined the possibility of increasing the lead-times associated to the runoff forecasting, since traditional warning systems based on rainfall observations do not provide the timely predictions required to implement the expected precautionary civil protection measures (Siccardi 1996). In western Mediterranean, recent efforts in this issue have focused on quantifying rainfall amounts from radar (Dolciné et al. 2001), since from these estimations, rainfall-runoff models can provide forecasts with lead-times ranging from <1h (Brémaud and Pointin 1993) to a few hours depending on the rainfall types (Conway and Browning 1988; Bellon and Zawadzki 1994; Hardaker et al. 1994). However, the only way to gain additional lead-time in runoff forecasting is to have rainfall information ahead of its occurence. One way in which this can be accomplished is by translating mesoscale model rainfall forecasts into runoff forecasts (Anderson et al. 2002; Ferraris et al. 2002). The feasibility of real-time forecasting over the Spanish Mediterranean area using the capabilities of a hydrological model forced by a mesoscale atmospheric model becomes one of the main issues of the present study.

The 10 June 2000 flash-flood event in Catalonia (northeast Spain) is a good example of the catastrophic effects of a rapid and sudden flow increase in a short time period. The region was affected by a convective rainfall episode which affected many internal catchments of the region and produced serious material and human damages. The feasibility of hydro-meteorological forecasting model strategies will be examined for this event. Specifically, the study is centered on the Llobregat basin, with a drainage area of 5040 km^2. The first objective of the study is to reproduce the hydrological response to the flash-flood event using the HEC-HMS runoff model. An independent sample of events is used to calibrate the HEC-HMS in terms of soil behaviour (losses and imperviousness), which exerts a fundamental role over the runoff volume for the episode, and flood wave celerity in the main channels of the catchment, an important factor owing to the high flow velocities. In order to optimize the rainfall-runoff model set up, the effects of diverse

spatial and temporal scales of the rainfall field on the simulated basin response have been quantified.

The second objective of the study is to test the appropriateness of the aforementioned atmospheric driven runoff simulations as a methodology for obtaining 12-48 hours forecasts of these extreme events, which would greatly expand the time necessary for emergency management procedures. In particular, the HEC-HMS runoff model is forced with mesoscale rainfall forecasts derived from MM5 simulations initialized with meteorological grid analyses from the American Center for Environmental Prediction (NCEP) and the European Center for Medium Range Weather Forecasts (ECMWF). The third objective consists of assessing the sensitivity of the Llobregat basin to the inherent uncertainties of some aspects of the hydro-meteorological forecasting chain (Ferraris et al. 2002; Castelli 1995; Murphy 1993). An ensemble of MM5 simulations with small shifts and variations of intensity of the precursor upper-level synoptic scale trough is designed for this purpose. With this method, it is possible to assess the effects on the hydrological response due to relatively moderate spatial and temporal errors of the forecast rainfall field.

The rest of this chapter consists of a brief description of the study area (section 1.3); and a brief description of the hydro-meteorological episode (section 1.4). In chapter 2, section 2.1 describes the hydrological tools used for the basin characterization, the methodology followed for the calibration and evaluation of the rainfall-runoff model and the analysis of the sensitivity to the spatio-temporal scales of the input rainfall field; and section 2.2 contains the meteorological tools applied to forecast the rainfall event and to design the ensemble of perturbed mesoscale simulations. Chapter 3 presents and discusses the results; and chapter 4 provides an assessment of the methodology which includes future directions for later development of the system.

1.3.1 Overview of the Llobregat basin

The Llobregat basin is the most important of the internal hydrographic catchments in Catalonia (fig. 1.4a) in terms of size, river length, mean flow and population living inside. It is composed of the Llobregat river and its main tributaries, the Anoia and the Cardener. Llobregat basin extends from the Pyrenees, with heights over 3000 meters, through the Pre-Pyrenees, constituted by a band of folded mesozoic materials, and crossing the central depression, formed by tertiary materials more or less eroded, with a height transition from 750 meters in the Pre-Pyrenees to 200 meters in the pre-coastal range. The last section of the river crosses the Mediterranean orographic systems, formed by two mountainous alignments almost parallel to the coast line: the pre-coastal range formed by varied morphological mounts (e.g. Montseny (1712 m), Montserrat (1236 m) and Serra del Cardó (942 m)) and the coastal range, consisting of small altitude mountains (e.g. Montnegre (759 m), Collserola (512 m) and Garraf (660 m)) (fig. 1.4b). The basin has a drainage area of 5040 km^2 and a maximum length close to 170 km.

Furthermore, the hydrographic catchment is divided into a wide range of climatic areas owing to the diversity of the pluviometric records depending on the altitude. Annual accumulated rainfall in the Llobregat basin can range from quantities exceeding 1000 mm in the Pyrenees (over 1000 meters), 700 mm over Pre-Pyrenees (with elevations comprised between 600-1000 meters) and 500 mm for altitudes below 500 meters. The rainfall regime is typical of the mediterranean areas, with most of heavy rainfall episodes occuring mainly in autumn, with occassional episodes in the spring and the summer. These daily rainfall episodes can represent a large fraction of the annual amounts.

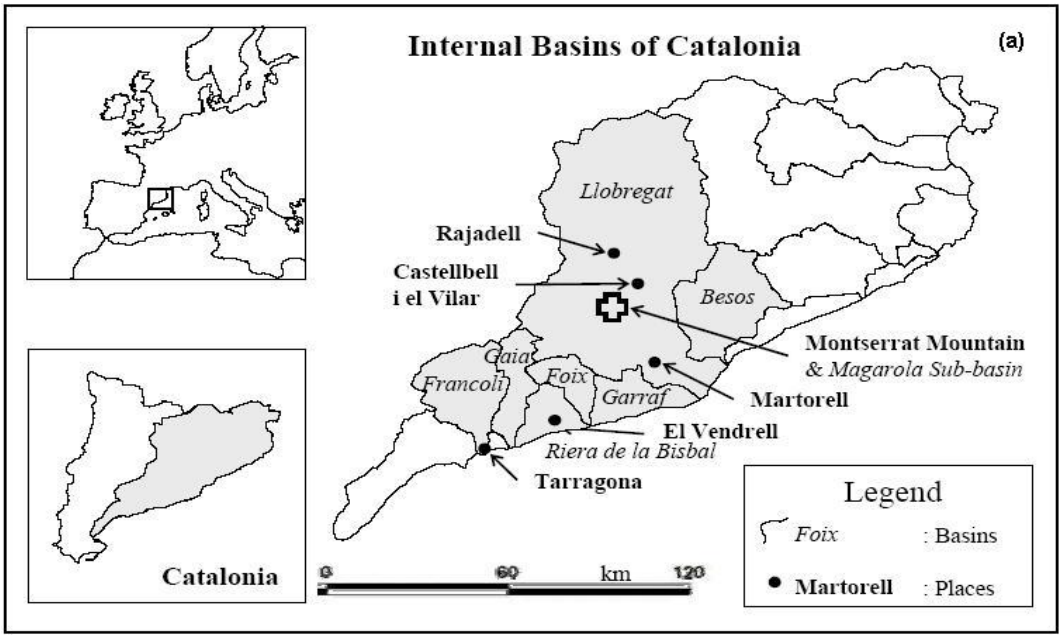

Figure 1.4: (a) Geographical location of the Internal Basins of Catalonia (IBC) where the Montserrat flash-flood event was produced. Several catchments (shaded) and locations affected by the episode are indicated. (b) The Catalan topography with a depiction of the main mountainous systems and rivers (Montserrat mountain and Llobregat river are indicated)

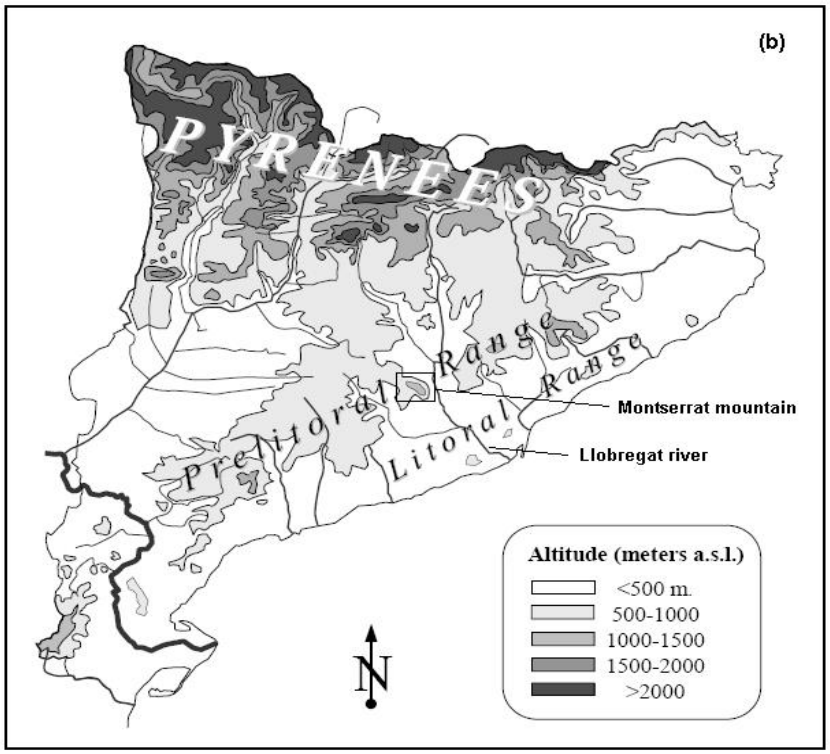

1.3.2 The rain and stream gauge networks

On 10 June 2000, heavy rainfall took place over the northeastern part of Spain and the most intense episode affected the whole of the Internal Basins of Catalonia (IBC; fig. 1.4a). The analysis of the pluviometric evolution of the episode used 5-minute rainfall data recorded at 126 stations inside the IBC and distributed over an area of 16000 km^2 (fig. 1.5). These stations belong to the Automatic Hydrological Information System (SAIH) network of the Catalan Agency of Water (ACA). Out of the 126 stations, about 40-50 lie inside the Llobregat basin or near its boundaries.

Runoff in the Llobregat basin was recorded in five flow gauges (fig. 1.6) located in: (i) Súria town, on the Cardener river, with a dranaige area of 940 km^2 and elevation from 250 m at gauge level to 2350 m in the Pyrenees; (ii) Sant Sadurní d'Anoia city, on the Anoia river, with a drainage area of 736 km^2 and elevations from 125 m at gauge level to 850 m at headwater; and (iii) Castellbell (3340 km^2), (iv) Abrera (3587 km^2) and (v) Sant Joan Despí (4915 km^2) towns along the Llobregat river. During the episode, 5-minute runoff

measurements were collected, jointly with the rainfall records, for the SAIH database.

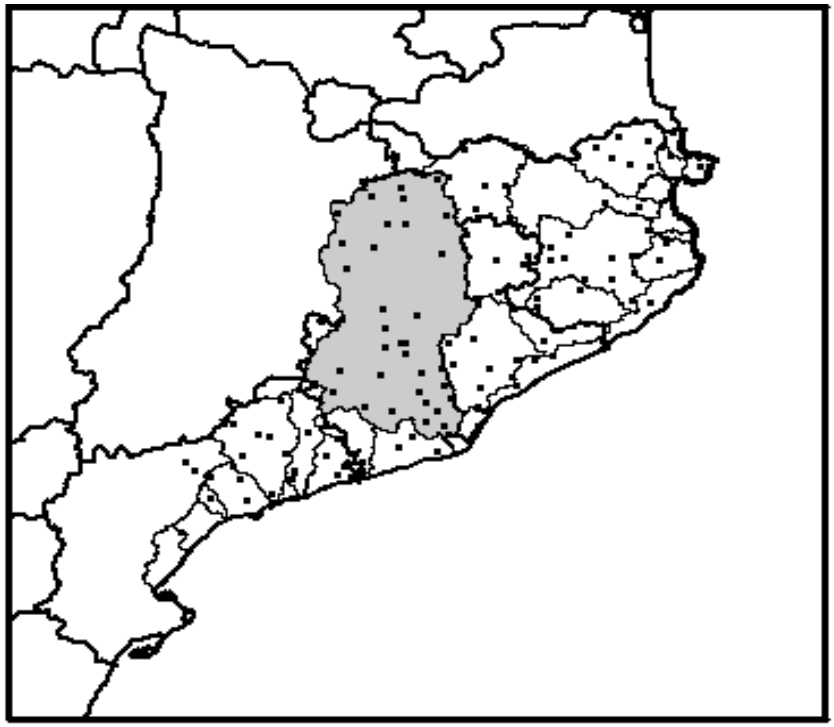

Figure 1.5: Distribution of the rain-gauges from the Automatic Hydrological Information System (SAIH) in the IBC. It includes a total of 126 automatic rainfall stations distributed over an area of 16000 km^2 (Llobregat basin is enhanced).

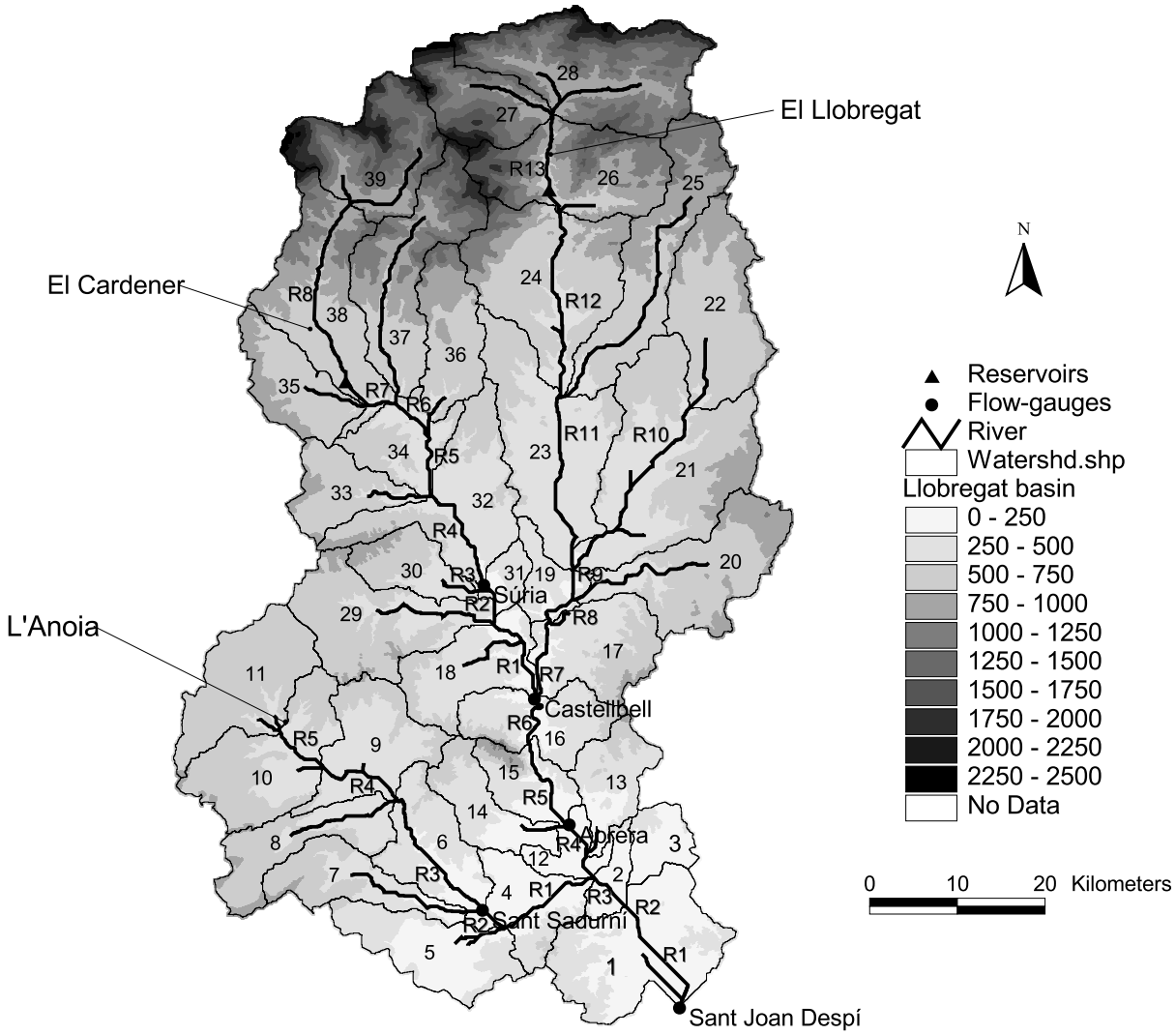

Figure 1.6: Digital terrain model of Llobregat river basin. It has a cell size of 50 m and displays the basin division (numbered), tributaries, stream-gauges (circles) and reservoirs (triangles) mentioned in the text.

1.4 Description of the Montserrat flash-flood episode

As widely described in Martín et al. (2006), this episode was characterized by the entrance of an Atlantic low-level cold front and an upper-level trough that contributed to the generation of a mesoscale cyclone in the Mediterranean Sea east of mainland Spain. This mesoscale cyclone advected warm and moist air toward Catalonia from the Mediterranean Sea. Then, the convergence zone between the easterly flow and the Atlantic flow as well as the complex orography of the region were shown to be involved in the triggering and organization of the convective systems which remained quasi-stacionary. Therefore, heavy rainfall on 10 June 2000 lasted about six hours, from 02:00 to 08:00 local time (see fig. 1.7; LT corresponds to UTC plus 2h).

The consistent extraordinary rise of the Catalonia internal river basin flow regimes (e.g. El Llobregat, El Besós, El Francolí and La Riera del Bisbal; see fig. 1.4a for locations) produced serious damages. Some of the most notable disasters consisted of the partial destruction of the infrastructure of Montserrat's Monastery (720 m) and some roads connecting with this mountainous area; the collapse of some bridges and sections in the plain roadway; and the flooding of residential zones with the attendant destruction of some dwellings, especially in the tourist municipality of El Vendrell (fig. 1.4a). As a consequence, about 500 people had to be evacuated from the monastery and the episode caused five fatalities and material losses estimated at about 65 million euros.

The most remarkable hydro-meteorological feature of this case, known as the 'Montserrat' flash-flood event for its impact upon Montserrat's mountain, was the high intensity of the sustained rainfall, which accumulated hourly quantities above 100 mm and a six-hour maximum up to 200 mm. Figures 1.8a and b depict, respectively, the radar image of the lowest CAPPI (constant altitude plan position indicator) at 04:00 LT and the cumulative rainfall distribution in the internal catchments from 23:00 LT on 9 June to 23:00 LT on 10 June. The maximum amounts were observed in the basin of the Llobregat river, with 224 mm in the town of Rajadell. Up to 134 mm were observed at Bisbal del Penedés town, in the basin of the Riera de Bisbal, of which above 100 mm occurred in less than 2

hours. Values exceeding 100 mm were also observed in the basins of the Francolí, Gaià, and Foix (Llasat et al. 2003; see fig. 1.4a for locations).

Focusing on the Llobregat basin (fig. 1.6), the maximum flow discharge observed at Súria was 260 m^3 s^{-1} at 12:25 LT with a time to peak of 6h (fig. 1.9a, black solid line). In the Anoia affluent, the maximum observed flow stage was close to 2.7 meters, with an associated peak discharge of 270 m^3 s^{-1} at 06:45 LT, and a time to peak of about 2 hours (fig. 1.9b). This was the first river which received the consequences of the event from 01:30 until 06:00 LT on 10 June. Around 03:00 LT, the rainfall extended to the entire Llobregat river basin, lasting for four hours. As a consequence, 5-minute intensites exceeded 120 mm per hour from 03:00 to 05:30 LT, with the highest values over the Llobregat basin occurring between 04:00 and 07:00 LT (fig. 1.8a). In Castellbell town, an increase on the flow stage was observed above 4.5 meters with several peak discharges, the maximum of these reaching 1000 m^3 s^{-1} at 08:00 LT with an associated time to peak close to 1h and 40 minutes (fig. 1.9c). In Abrera, a town sited approximately 15 km downstream, the maximum peak discharge was close to 1200 m^3 s^{-1} (at 12:50 LT; fig. 1.9d). Finally, at Sant Joan Despí city, near the Llobregat river mouth where the last river gauge is installed, the maximum peak discharge was up to 1400 m^3 s^{-1} at 10:15 LT with a timing close to 2h and 20 minutes (fig. 1.9e). These short response times shown by the hydrographs (see figure 1.9) indicate substantial flow velocities in the subbasins induced by the high rainfall rates, and discharge that propagated very rapidly downstream (9 km h^{-1} on average).

The Spanish Center for Studies and Experimentation on Public Works (CEDEX) has issued, in the framework of a report on flood plain management, the return periods corresponding to certain runoff thresholds for several national catchments. For the Llobregat basin, the associated return period for an outflow of 1025 m^3 s^{-1} is 10 years, whereas for a peak discharge of 1600 m^3 s^{-1} the recurrence interval is 20 years (Menéndez 1998). These estimations emphasize the notable magnitude of the Montserrat event (1400 m^3 s^{-1}). The probability of suffering a similar catastrophic episode in the Llobregat basin is relatively low, but it must be emphasized that several hazardous episodes of different

magnitudes and spatial scales are produced every year over the Spanish Mediterranean regions. In addition, future climate change scenarios and their possible impact on these type of events have to be taken into account. Some authors have indicated an increase in the probability of heavy rainfall episodes in several parts of the world (Groisman et al. 1999), and a paradoxial increase of extreme daily rainfall in spite of a decrease in total values has been observed already in the Mediterranean basin (Alpert et al. 2002).

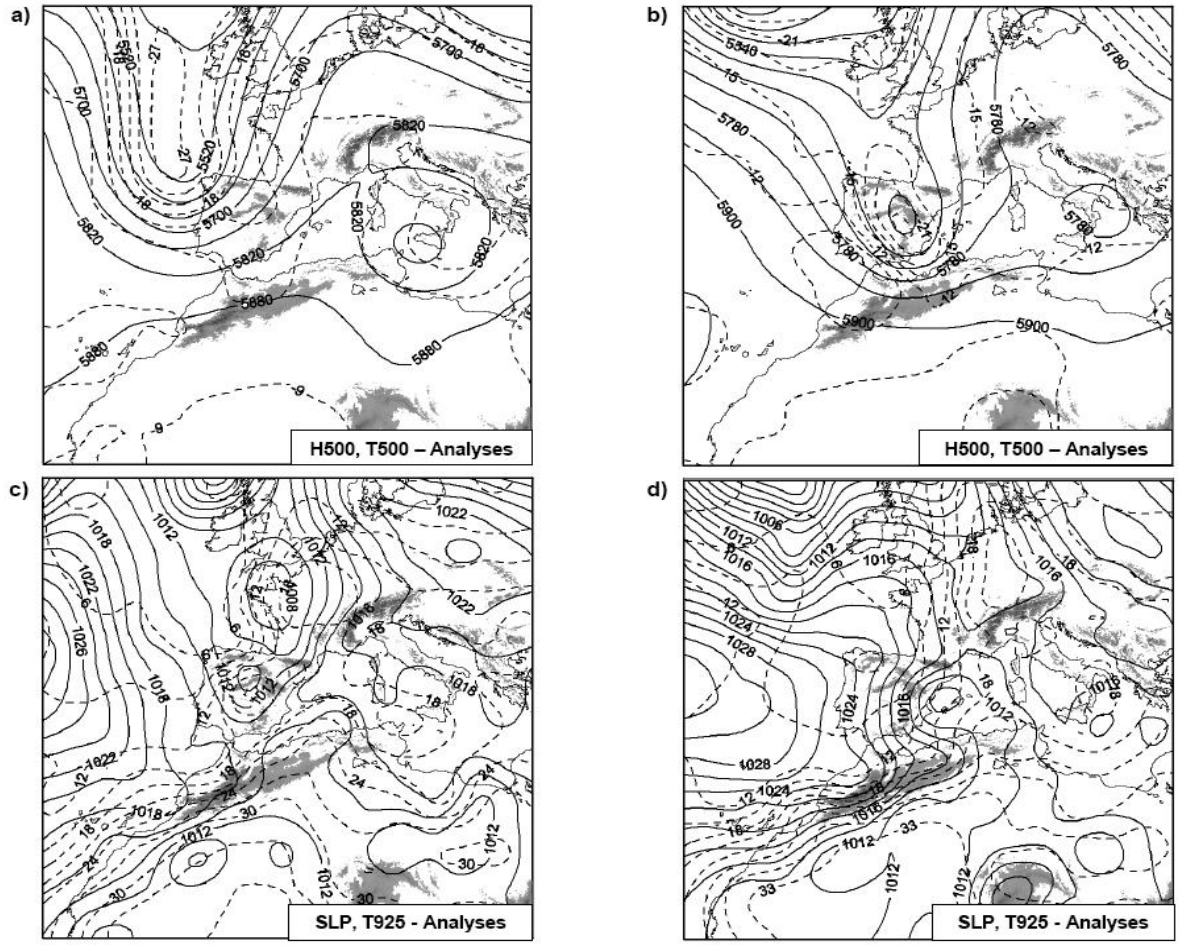

Figure 1.7: NCEP analyses maps. **(Top)** Geopotential height at 500 hPa (continuous line, in gpm) and temperature at 500 hPa (dashed line, in ^{0}C): **(a)** at 0000 UTC 9 June 2000; and **(b)** at 0000 UTC 10 June 2000. **(Bottom)** Sea level pressure (continuous line, in hPa) and temperature at 925 hPa (dashed line, in ^{0}C): **(c)** at 0000 UTC 9 June 2000; and **(d)** at 0000 UTC 10 June 2000. Main orographic systems are highlighted.

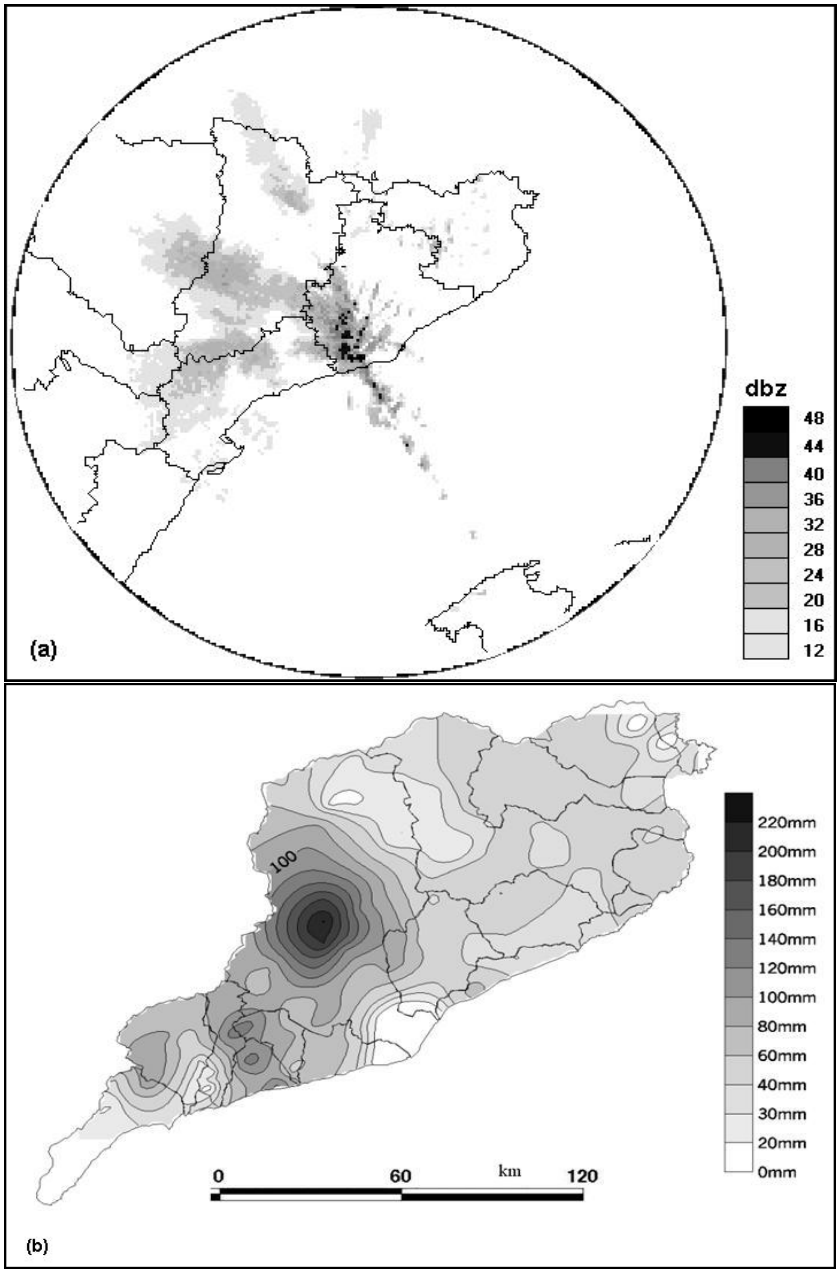

Figure 1.8: (a) CAPPI reflectivity at 1.2 km altitude recorded by the Barcelona radar at 04:00 LT on 10 June 2000. (b) SAIH-derived analysis of accumulated rainfall over the IBC during the 'Montserrat' episode.

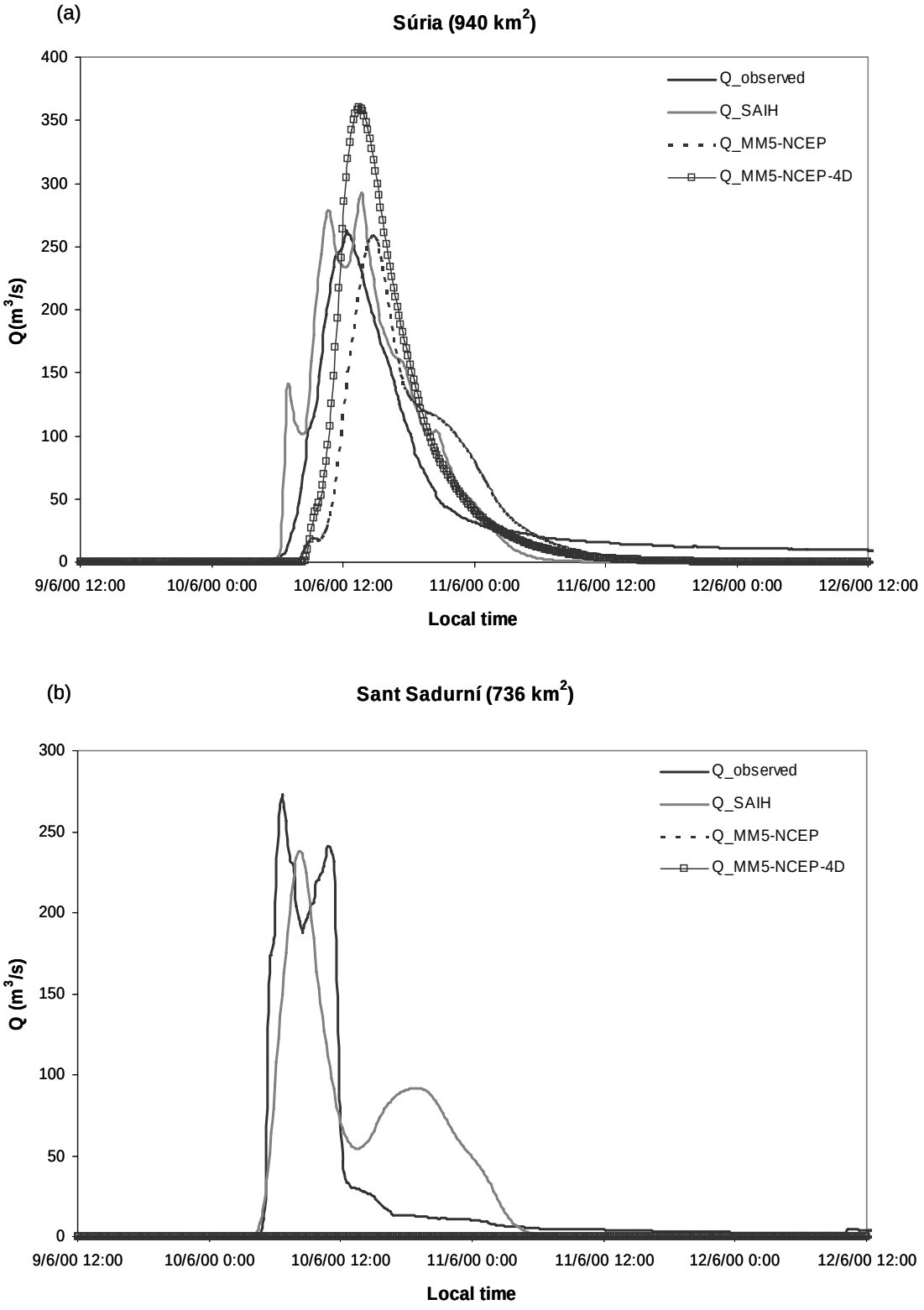

Figure 1.9: Observed, SAIH rain-gauge driven, and MM5-NCEP simulation driven runoff discharge at: (a) Súria, (b)Sant Sadurní, (c) Castellbell, (d) Abrera and (e) Sant Joan Despí.

(c)

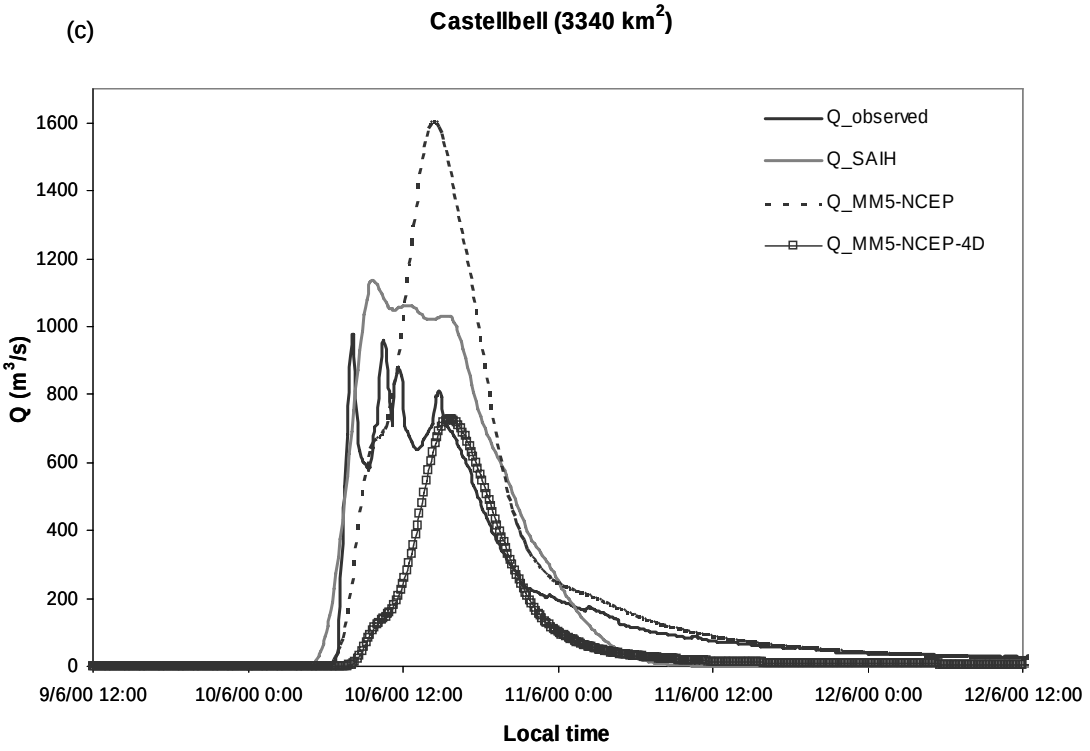
Castellbell (3340 km2)
Q_observed
Q_SAIH
Q_MM5-NCEP
Q_MM5-NCEP-4D
Q (m3/s)
1600
1400
1200
1000
800
600
400
200
0
9/6/00 12:00
10/6/00 0:00
10/6/00 12:00
11/6/00 0:00
11/6/00 12:00
12/6/00 0:00
12/6/00 12:00
Local time

(d)

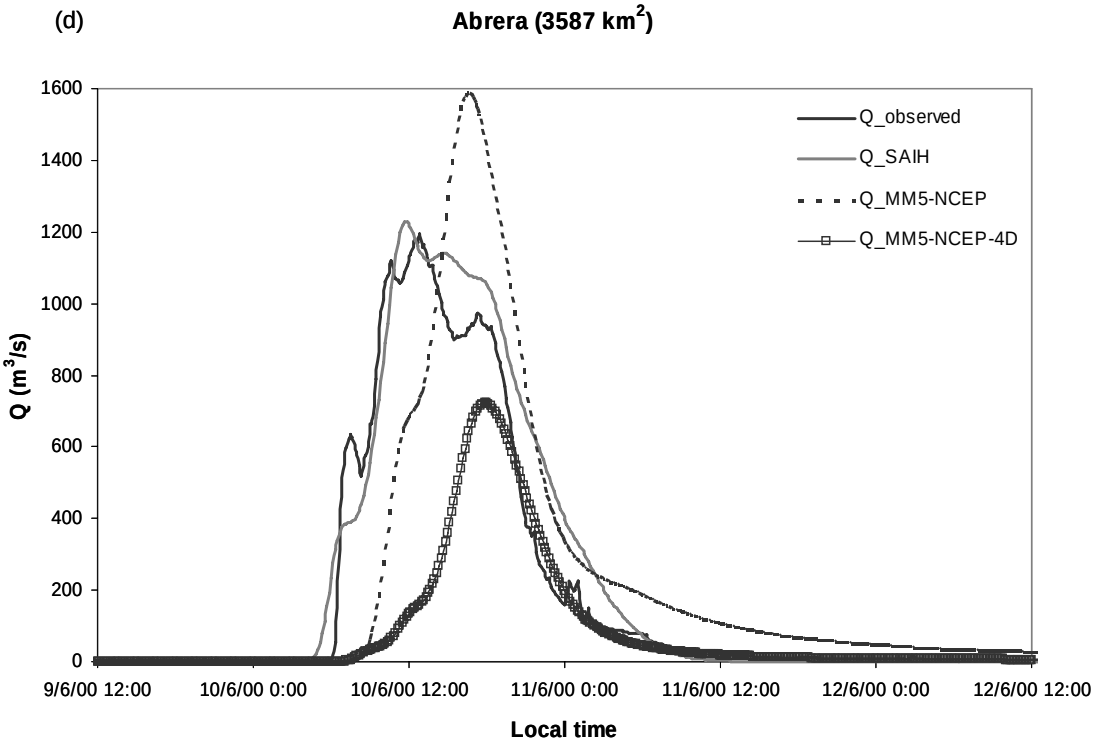
Abrera (3587 km2)
Q_observed
Q_SAIH
Q_MM5-NCEP
Q_MM5-NCEP-4D
Q (m3/s)
1600
1400
1200
1000
800
600
400
200
0
9/6/00 12:00
10/6/00 0:00
10/6/00 12:00
11/6/00 0:00
11/6/00 12:00
12/6/00 0:00
12/6/00 12:00
Local time

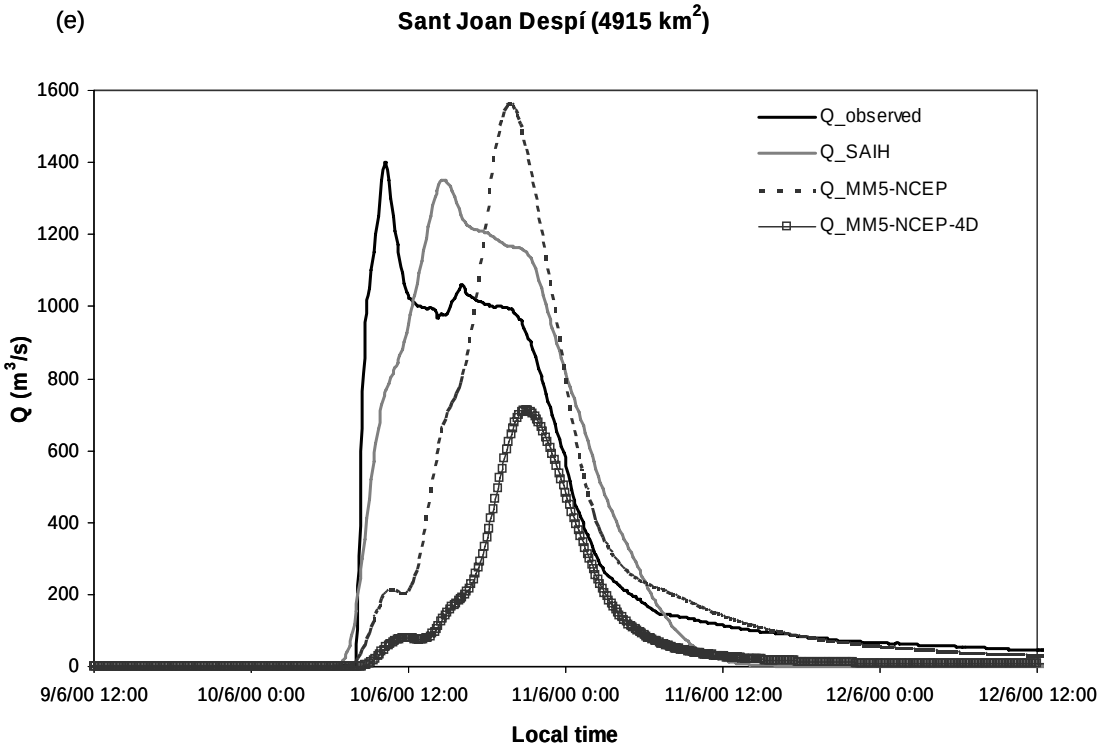
(e)
Sant Joan Despí (4915 km2)
1600
1400
1200
1000
800
600
400
200
0
Q (m3/s)
9/6/00 12:00
10/6/00 0:00
10/6/00 12:00
11/6/00 0:00
11/6/00 12:00
12/6/00 0:00
12/6/00 12:00
Local time
Q_observed
Q_SAIH
Q_MM5-NCEP
Q_MM5-NCEP-4D

Chapter 2

HYDRO-METEOROLOGICAL TOOLS

2.1 Hydrological tools

2.1.1 Rainfall-runoff model and input data

This study is carried out using the HEC-HMS rainfall-runoff model, developed by the US Army Corps of Engineers (USACE-HEC 1998). HEC-HMS utilizes a graphical interface to build a semi-distributed watershed model and to set up rainfall and control variables for the simulation. Figure 1.6 depicts the digital terrain model for the Llobregat basin -with a cell resolution of 50 meters- together with the main watercourses and its tributaries, the considered division in subbasins and the location of the available river gauges. After the analysis presented in section 2.1.3, the basin is divided in 39 subwatersheds with an average size of 126 km^2 and an extension of 4915 km^2 upstream from Sant Joan Despí, where the last flow-gauge is installed.

HEC-HMS is forced using a single hyetograph for each subbasin. Rainfall spatial distributions were first generated from 30-min, 1-h and 3-h accumulated values at SAIH rain-gauges (see section 2.1.3) using the kriging interpolation method with a horizontal grid resolution of 1 km. Then, temporal rainfall series were calculated for each subbasin as the areal average of the gridded rainfall within the subcatchment. The same method-

ology is used to assimilate forecast rainfall fields in HEC-HMS (chapter 3), except that atmospheric model grid point values are used instead of SAIH observations.

2.1.2 Theoretical background and basin calibration

(a) SCS method for abstractions

The excess rainfall, or effective rainfall, is that rainfall which is neither retained on the land surface nor infiltrated into the soil. After flowing across the basin surface, excess rainfall becomes direct runoff at the basin oulet. The difference between the observed total rainfall hyetograph and the excess rainfall hyetograph is termed abstractions or losses. The hydrologic model calculates the excess precipitation volume by subtracting from rainfall the water volume that is lost through interception, infiltration, storage, evaporation and transpiration. The loss rate is calculated using the Soil Conservation Service Curve Number (SCS-CN; see, for instance, US Department of Agriculture 1986). This method assumes the storm runoff volumes, P_e, to be proportional to the rainfall volumes, P, exceeding an initial abstraction threshold, I_a, through the ratio of the accumulated infiltration, F_a, to the potential maximum storage capacity, S.

$$P_e = \frac{F_a}{S} \cdot (P - I_a) \text{ for P}>I_a\text{; 0, otherwise.}$$

The initial abstraction, I_a, represents the maximum capacity of interception and depression storages. Standard procedures, tested on a wide experimental basis, suggests that $I_a \simeq 0.2 \cdot$S should be adopted when field measurements for the watershed under study are not available for the initial abstractions. With this assumption together with the continuity equation that for P$>I_a$ states that

$$P = P_e + I_a + F_a$$

the cumulative volume of stormflow becomes nonlinearly related to the excess rainfall volume (P-I_a):

$$P_e = \frac{(P - 0.2S)^2}{P + 0.8S}$$

which is a function of cumulative rainfall, soil cover, land use and antecedent moisture (see fig. 2.1; Chow et al. 1988, Bacchi et al 2002).

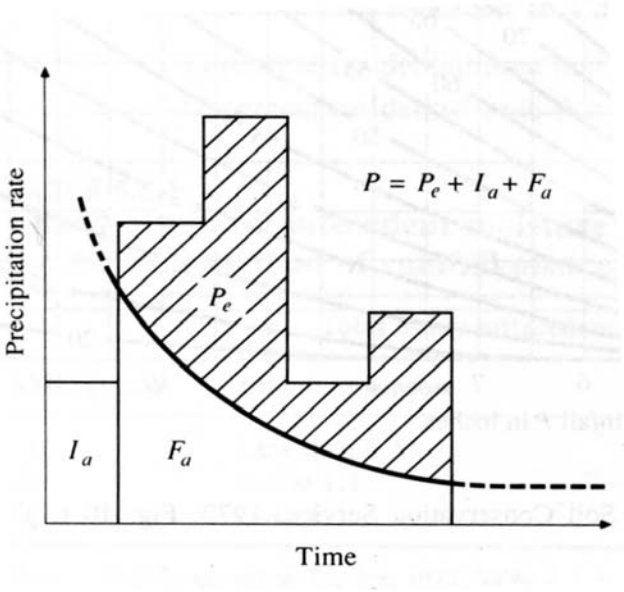

Figure 2.1: Variables in the SCS method of rainfall abstractions.

The maximum retention and the basin characteristics are related through an intermediate parameter, the curve number (CN) and according the SCS formulation for normal antecedent moisture conditions:

$$S = \frac{25400 - 254CN}{CN}$$

where the CN values can range from 100 for water bodies to approximately 30 for permeable soils with high infiltration rates. The SCS-CN model has been tested on several experimental areas and river basins worldwide and, in Catalonia has been adopted by ACA in their technical studies (ACA 2001, 2003). The SCS-CN model has the advantage that with a single parameter (the storage capacity) it reproduces two phenomena that

are systematically observed during floods: an initial loss of rain and an increase in the efficiency of the basin in producing runoff as a response to the rainfall input (Ranzi et al. 2003).

(b) Unit hydrograph

In order to convert rainfall excess into direct runoff, it is applied the fundamental assumption that the watersheds respond as linear systems. Then, the relationship between storage, inflow and outflow is such that it leads to a linear differential equation. The hydrologic reponse of such systems can be expressed in terms of an impulse response function (IRF) through a so-called Convolution Equation. This implies that the proporcionality principle applies so that effective rainfall intensitities of different magnitude produce basin responses that are accordingly scaled. It also implies that the superposition principle applies so that the responses of several different storms can be superimposed to obtain the composite response of the catchment, which are implicit in the convolution equation (see fig. 2.2).

The IRF of a linear system represents the response of the system to an instantaneous impulse of unit volume applied at the origin in time (t=0). The response of continuous linear systems can be expressed, in the time domain, in terms of the impulse response function via the convolution integral as follows,

$$Q_t = \int_0^t I_e(\tau) u(t-\tau) d\tau$$

where $u(t)$ is the impulse response function of the system.

When dealing with hydrologic systems, $u(t)$ represents the instantaneous unit hydrograph (UH), and Q_t and $I_e(t)$ represent direct runoff and excess precipitation, respectively. Thus, an unit hydrograph represents the response of watershed, discharge at its outlet as a function of time, to a unit volume of precipitation occuring instantaneously at time t=0.

When the effective rainfall is given as a hyetograph, that is, as a sequence of M rainfall pulses of the same duration, Δt, the corresponding direct runoff hydrograph can

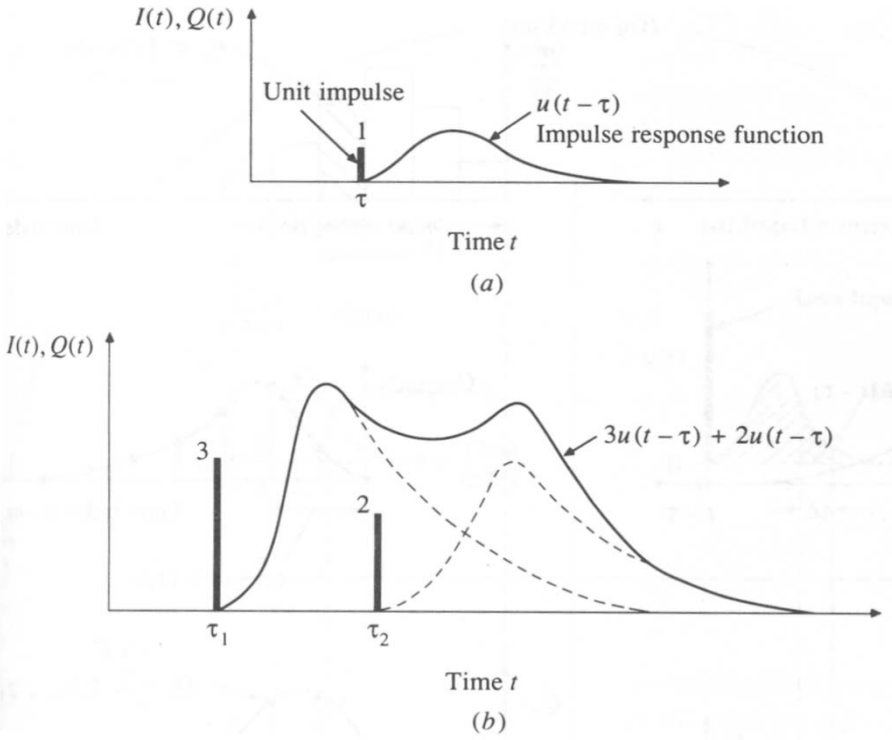

Figure 2.2: Responses of a linear system to impulse inputs. (a) Unit impulse response function. (b)The response to two impulses is found by summing the individual response functions.

be expressed as a discrete convolution equation of the rainfall hyetograph and a unit hydrograph (figs. 2.3 and 2.4),

$$Q_n = \sum_{m=1}^{m^*} P_m U_{n-m+1} \quad \mathrm{m}^* = min(n, M)$$

$$Q_n = Q(n\Delta t) \quad \mathrm{n}=1,2,...,\mathrm{N}$$

$$P_m = \int_{(m-1)\Delta t}^{m\Delta t} I(\tau)dt \quad \mathrm{m}=1,2,...,\mathrm{M}$$

where P_m is the volume of the m^{th} effective rainfall pulse. The value of the system output, Q_n, in the n^{th} time interval ($t = n\Delta t$) is the instantaneous value of the flow rate at the end of the n^{th} time interval. The effect of an input pulse duration Δt beginning at time $(m-1)\Delta t$ on the output time $t = n\Delta t$ is measured by the value of the unit pulse response function which can be represented on a discrete time domain as a sample function U_{n-m+1}.

Then, the discrete convolution equation allows the computation of direct runoff Q_n given excess rainfall P_m and the unit hydrograph U_{n-m+1} (Chow et al., 1988).

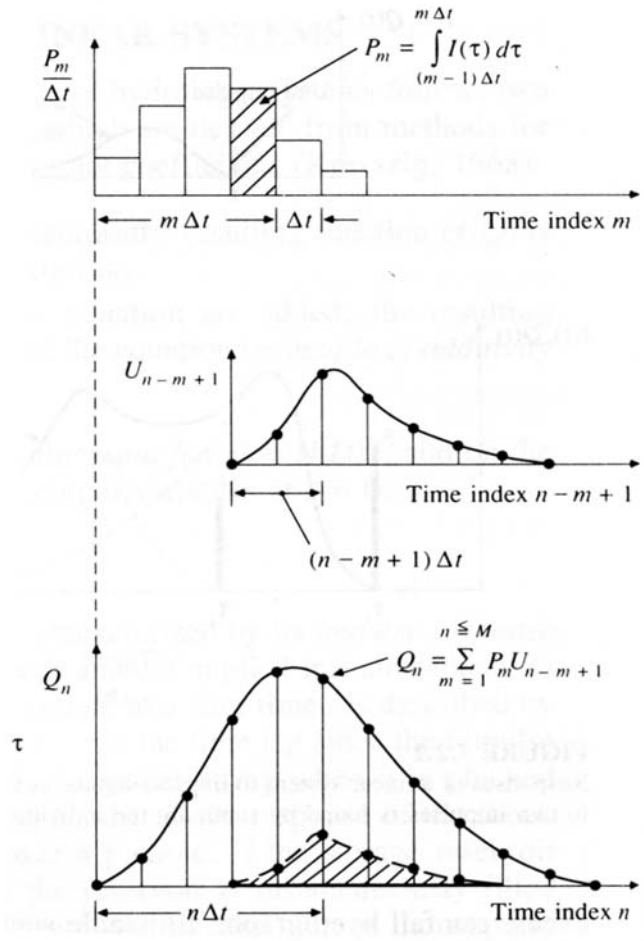

Figure 2.3: Scheme of the discrete convolution.

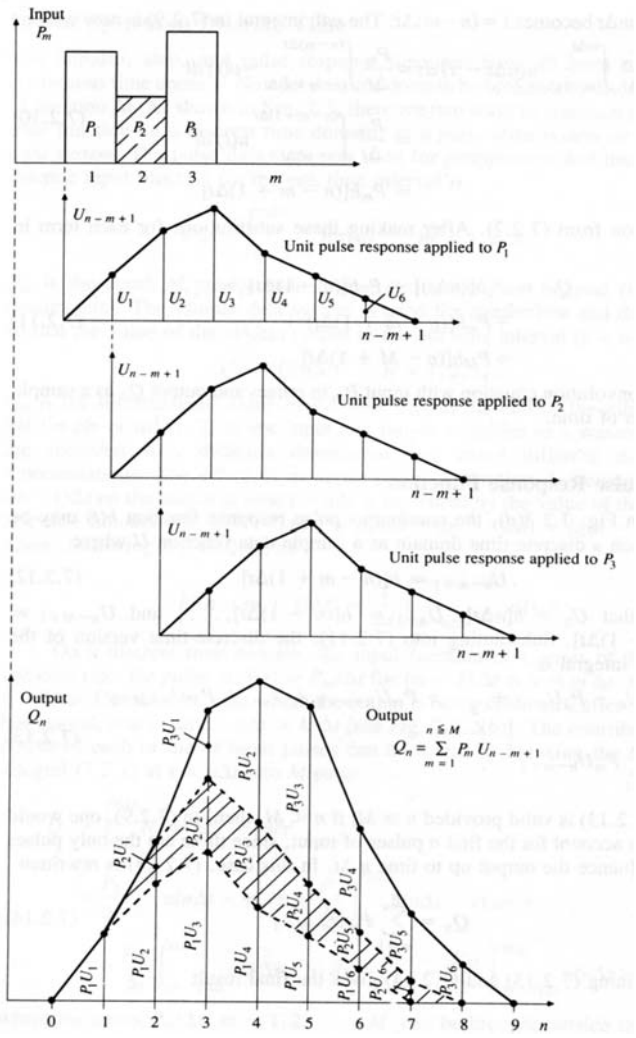

Figure 2.4: Application of the discrete convolution equation to the output from a linear system.

A synthetic unit hydrograph (UH) provided by SCS is used to convert rainfall excess into direct runoff on a watershed. The discharge is expressed by the dimensionless SCS-UH as the ratio of discharge, U_t, to peak discharge, U_p, and the time by the ratio of time t to the time of rise of the unit hydrograph, T_p. Given the peak discharge and the lag time for the duration of the excess rainfall, the unit hydrograph can be estimated from the synthetic dimensionless hydrograph for the given basin. Figure 2.5 shows such a dimensionless hydrograph prepared form the unit hydrographs of a variety of watersheds where the time is in hours and the discharge in $m^3s^{-1}cm^{-1}$. It can be shown that

$$U_p = C\frac{A}{T_p}$$

in which C=2.08 in the international system and A is the drainage area in square kilometers. The time of peak is related to the duration of excess precipitation as

$$T_p = \frac{\Delta t}{2} + t_{lag}$$

in which Δt is the excess rainfall duration and t_{lag} is the basin lag, defined as the time difference between the centroid of rainfall excess and the UH peak discharge. Following CEDEX recommendations, based on previous SCS,

$$t_{lag} = 0.35T_c$$

where the time of concentration of the basin, T_c (in hrs), is calculated applying the Témez empirical formula (Témez, 1978):

$$T_c = 0.3(\frac{L}{j^{0.25}})^{0.76}$$

and L is the channel length (in km) and j the channel mean slope (in m/m). When the lag time is specified, it can be obtained the time of UH peak and the UH peak (Chow et al. 1988; USACE-HEC 2000).

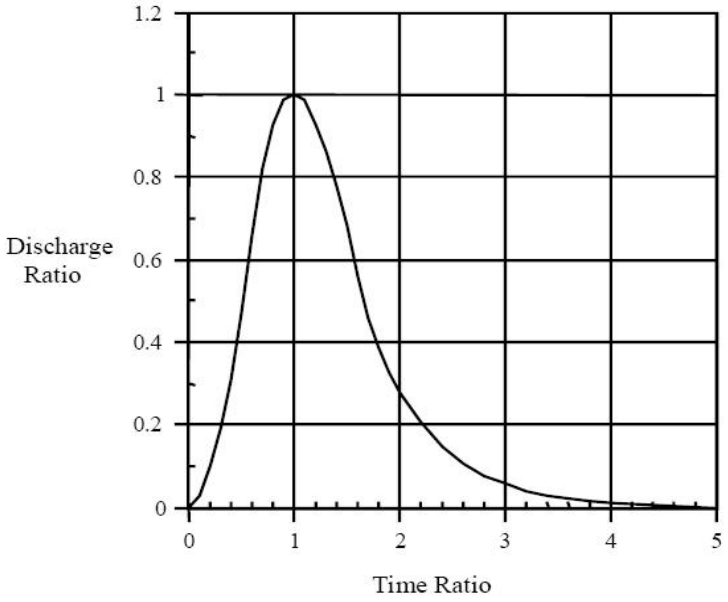

Figure 2.5: Soil Conservation Service dimensionless unit hydrograph.

(c) Flow routing and kinematic wave approximation

Flow routing is a procedure to determine the time and magnitude of the flow -the flow hydrograph- at a point in the watercourse from known hydrographs at one o more points upstream and it is the physical process to define the discharge hydrograph evolution along the river. As flood waves travel downstream they are attenuated and delayed. That is, the peak flow of the hydrograph decreases and the time base and the time to peak of the hydrograph increases. The shape of the outflow hydrograph depens upon diverse factors as the channel geometry and roughness, bed slope, length of the channel reach and the initial and the boundary flow conditions (fig. 2.6).

For the hydrologic routing, the inflow at the upstream end, I(t) and the outflow at the end of the watercourse, Q(t), are related by the principle of mass conservation:

$$I(t) - Q(t) = \frac{dS}{dt}$$

which requires that the difference between the two flows has to be equal to the time

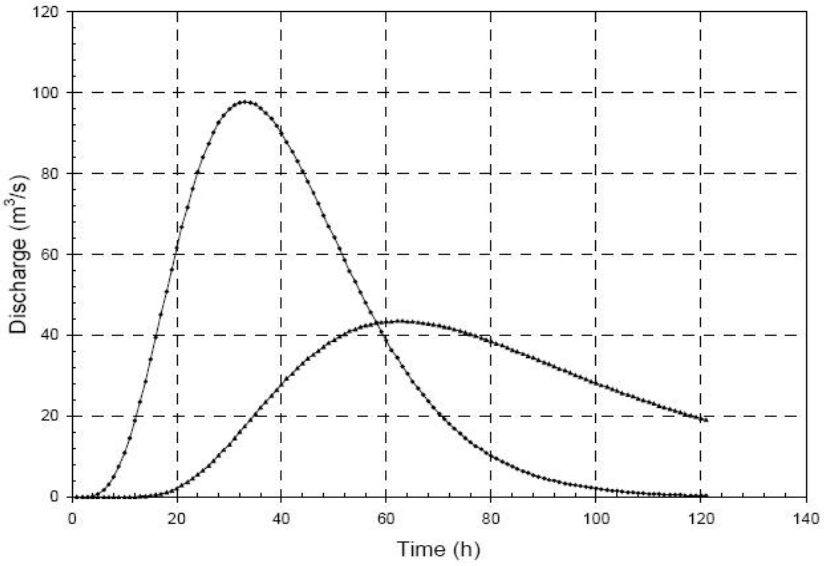

Figure 2.6: Inflow and outflow hydrographs for the Muskingum routing.

rate of change of the storage within the reach, S. Here Q and S are unknown. A second relationship, the storage function is needed to relate I, Q and S. In general the storage function may be written as a function of I, Q and their derivatives (although it also depens on the characteristics of the channel reach):

$$S = f(I, \frac{dI}{dt}, \frac{d^2I}{d^2t}, ..., Q, \frac{dQ}{dt}, \frac{d^2Q}{d^2t}, ...)$$

The mass conservation equation is solved in HEC-HMS using the finite difference method. Incorporating a finite-difference approximation for the partial derivatives yields

$$(\frac{I_{t-1} + I_t}{2}) - (\frac{Q_{t-1} + Q_t}{2}) = (\frac{S_t + S_{t-1}}{2})$$

where I_t is the inflow rate at the considered reach, Q_t is the outflow rate and S_t the storage rate (in m^3s^{-1}). The Muskingum model is used as hydrologic routing method (Chow et al. 1988, USACE-HEC 2000; see fig. 2.6). It models the storage function in a river channel by a combination of a wedge and a prism storages (fig. 2.7). The storage is defined as:

$$S_t = K[\chi I_t + (1 - \chi)Q_t]$$

where K is the travel time of the flood wave through the routing reach (in s) and χ a dimensionless weight ($0 \leq \chi \leq 0.5$). Storage in the reach is modeled as a sum of prism and wedge storage.

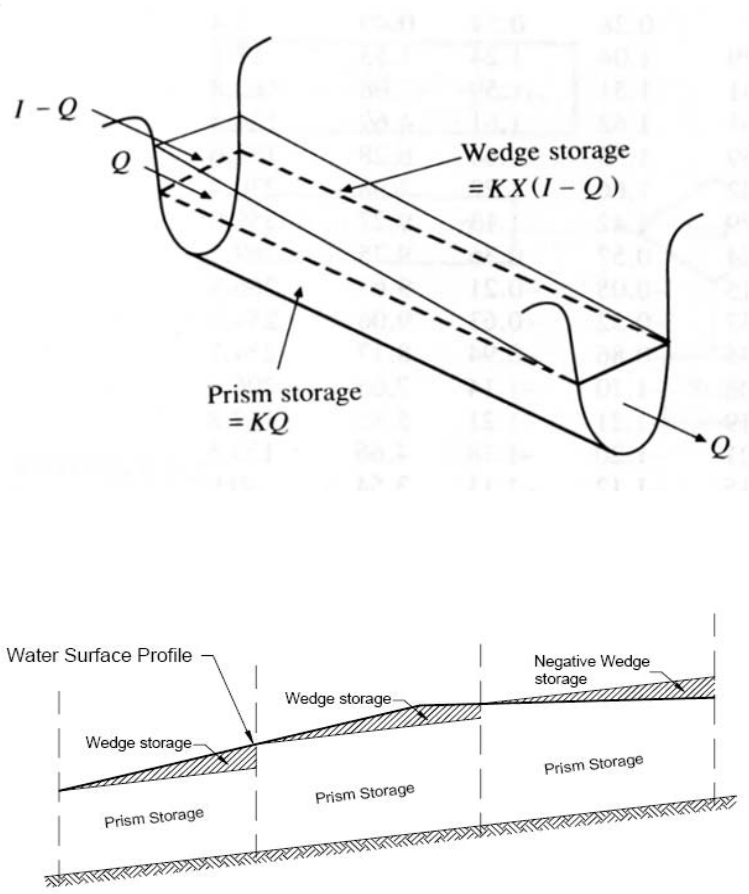

Figure 2.7: Prism and wedge storages in a channel reach.

Combining both equations:

$$Q_t = C_0 I_t + C_1 I_{t-1} + C_2 Q_{t-1} \text{ where}$$

$$C_0 = \frac{\Delta t - 2K\chi}{2K(1-\chi) + \Delta t}$$

$$C_1 = \frac{\Delta t + 2K\chi}{2K(1-\chi) + \Delta t}$$

$$C_2 = \frac{2K(1-\chi) - \Delta t}{2K(1-\chi) + \Delta t}$$

$$\text{where } C_0 + C_1 + C_2 = 1$$

In order to determine the value of K and χ on the basis of channel characteristics and flow rate in the channel must be used the equations of open channel flow.

The fundamental equations of open channel flow are the continuity and momentum equations. Together the two equations are known as the Saint-Venant equations or the dynamical wave equations. The continuity equation accounts for the volume of water in a reach of an open channel, including the flowing into the reach, the flowing out of the reach, and the stored in the reach. In one dimension, the conservative form of the equation is applicable at a channel cross section:

$$\frac{\partial Q}{\partial x} + \frac{\partial A}{\partial t} - q_l = 0$$

where Q is the flow entering at the upstream end of the channel, q_l is the lateral inflow per unit length of channel, x is the distance along the flow path, A is the average cross-sectional area and v_{lx} is the x-component of the mean velocity for the lateral inflow. Each of the terms in this equation describes inflow to, outflow from or storage in a reach of channel, a lake or pond, or a reservoir. The terms can be described as: $\frac{\partial Q}{\partial x}$ is the rate of change of channel flow with distance and $\frac{\partial A}{\partial t}$ the rate of change of mass stored.

The momentum equation accounts for forces that act on a body of water in a open channel. In simple terms, it equates the sum of gravitational force, pressure force and friction force to the product of fluid mass and acceleration. In one dimension, the equation is written for the conservative form as:

$$\frac{1}{A}\frac{\partial Q}{\partial t} + \frac{1}{A}\frac{\partial}{\partial x}\left(\frac{Q^2}{A}\right) + g\frac{\partial y}{\partial x} - g(S_o - S_f) - q_l v_{lx} = 0$$

where $\frac{1}{A}\frac{\partial Q}{\partial t}$ is the local acceleration; $\frac{1}{A}\frac{\partial}{\partial x}(\frac{Q^2}{A})$ is the convective acceleration; $g\frac{\partial y}{\partial x}$ is the pressure force term; gS_f is the friction force term; gS_o the gravity force term and $q_l v_{lx}$ is the momentum entering the main channel with the lateral inflow.

Althought the solution of the full equations is appropriate for all one-dimensional channel-flow problems, approximations of the full equations are adequade for typical flood routing needs. These approximations combine the continuity equation with a simplified momentum equation that includes only relevant and significant terms. For flash-floods, the momentum equation can be simplified to only contain the garvity and friction force terms. If this simplified momentum equation is combined with the continuity equation, the result is the kinematic wave approximation. Kinematic waves govern the flow when inertial and pressure forces are not important, then these terms are negligible in the momentum equation and the movement is described principally by the equation of continuity. The gravity and friction forces are balanced, so the flows does not accelerate appreciably. The energy grade line is parallel to the channel bottom and the flow is steady and uniform for a differencial length, dx. Then, the kinematic wave model is defined by the following equations, assuming that the lateral inflow is insignificant:

$$\frac{\partial Q}{\partial x} + \frac{\partial A}{\partial t} = 0$$

$$S_o = S_f$$

By combining the continuity and momentum equations:

$$\frac{\partial Q}{\partial t} + c_K \frac{\partial Q}{\partial x} = 0$$

which is the kinematic wave equation and it is accomplished that

$$K = \frac{\Delta x}{c_K} = \frac{\Delta x}{dQ/dA}$$

$$\chi = \frac{1}{2}(1 - \frac{Q}{Bc_K S_o \Delta x})$$

where c_K is the celerity corresponding to Q and B, and B is the width of the water surface. The energy gradient can be estimated with Manning's equation which can be written as:

$$Q = \frac{S_f^{1/2} A^{5/3}}{nP^{2/3}}$$

combined with the kinematic wave approximation it can be shown that:

$$K = \frac{5}{3} T_R$$

where T_R is the travel time through the subbasin and it is calculated using the Témez formulation. Finally to avoid instabilities in the computation iterations it is required that $0 \leq \chi \leq 0.5$ ($\chi \approx 0.2$ in natural streams) and it must be imposed to the iteration time the following condition:

$$2K\chi \leq \Delta t \leq K$$

(d) Reservoir modeling

A reservoir or detention pond mitigates adverse impacts of excess water by holding that water and releasing it at a rate that will not cause damage downstream. The structure stores water temporarily and releases it, either through the outlet pipe or over the emergency spillway. Thus, it limits the release of water during a flood event and it provides a method of emptying the pond after the event so that the reservoir can store future runoff. Outflow can be computed with the level-pool routing model (or also known as Modified Puls routing model). It solves recursively the following one-dimensional approximation of the mass conservation equation:

$$I_{avg} - Q_{avg} = \frac{\Delta S}{\Delta t}$$

in which I_{avg} is the average inflow during time interval, Q_{avg} the average outflow during time interval and ΔS the storage change. With a finite difference approximation, this can be written as:

$$(\frac{2S_{t+1}}{\Delta t} + Q_{t+1}) = (I_t + I_{t+1}) + (\frac{2S_t}{\Delta t} - Q_t)$$

All terms in the right side are known. The values of I_t and I_{t+1} are the inflow hydrograph ordinates. The values of Q_t and S_t are known at the t^{th} time interval. At t=0, these are the initial conditions, and at each subsequent interval, they are known from calculation in the previous interval. Therefore the quantity $(\frac{2S_{t+1}}{\Delta t} + Q_{t+1})$ can be calculated, since storage and outflow are related with the storage-outflow relationship. The computations

are repeated for successive intervals yielding the required outflow hydrograph ordinates (USACE-HEC 2000).

The Llobregat basin contains two reservoirs located in the upstream areas of the Cardener affluent and the Llobregat river (fig. 1.6). Therefore, these watercourses can not be modeled under the natural regime since the dams have an important hydrograph diffusion effect in the flood wave. The technical characteristics of both reservoirs -storage capacity, maximum outflow, maximum elevation and initial level- have been obtained from the aforementioned technical reports by ACA (a third reservoir exists in the Llobregat basin, but it has not been modeled since it is not considered in the technical reports). The detention ponds are modeled in HEC-HMS introducing a reservoir element that follows the elevation-storage-outflow relationship series which depends on the characteristics of the dam, the outlet and the spillway, besides the initial elevation of the water level.

(e) Calibration of the Llobregat basin

The last subsections have exposed some physical schemes used to model the runoff in HEC-HMS. The values of the parameters involved in these physical schemes can be estimated from several theoretical frameworks and various basin and channel properties. However, some of the parameters that are included in the study cannot be easily estimated by observations or field measurements. Furthermore, the high spatial and temporal variability associated with the infiltration mechanism plays a fundamental role in the great uncertainties which arise in the setting of the rainfall-runoff model's initial conditions. This implies that in order to maximize the model performance, the model should be carefully optimized before any application is carried out. This optimization process is best conducted by using rainfall observations to drive the model and comparing results with observed discharges. It is important to remark that the choice of the optimum model parameters is carried out on physically sound bases and it is designed to optimize the model representation of observed physical processes. This indeed increases both the model performance and its applicability to different studies.

Therefore if rainfall and streamflow observations are available, a calibration task must

be done. Calibration uses observed hydro-meteorological data in a systematic search of parameters that yield the best fit of the computed results to the observed runoff in an optimization process. Once the initial best estimation of the parameters is selected, the physical schemes included in HEC-HMS can be used with the observed boundary conditions (rainfall and upstream flow) to compute the output and to compare the computed and observed hydrographs. If the model does not fit the real hydrologic system in a realistic way, the parameters can be adjusted using determined algorithms, running the simulation and applying some methods of comparison again. The process is reiterative until the fit is satisfactory and then HEC-HMS will have obtained the optimal parameter values.

The calibration of the rainfall-runoff model is carried out using five episodes of similar extraordinary characteristics to our Montserrat case of study -which is used to evaluate the model-, selected from the period comprised between the deployment of the SAIH system (in 1996) and 2004 (table 2.1). Owing to the malfunction of the flow-gauge network for some of these episodes, the stream-gauges at Abrera and Sant Joan Despí are not available for all the cases (table 2.1), limiting to some extent the calibration of the lower Llobregat basin.

Flood events	***Simulation periods***	***Maximum observed rainfall (mm)***	***Maximum observed flow ($m^3\ s^{-1}$)***
16-19 Nov 1996	96 h	102.1	1250.0 (Despí)
16-19 Dec 1997	96 h	232.0	502.7 (Castellbell)
17-20 Oct 2001	96 h	84.5	254.4 (Despí)
03-06 Dec 2003	96 h	63.6	436.9 (Castellbell)
29-31 Aug 2004	72 h	178.3	313.5 (Castellbell)

Table 2.1: Summary of the episodes used for the calibration of the hydrologic model. Note that the observed flow at the basin outlet in Sant Joan Despí is not available for some of the cases.

Calibration of the infiltration parameters for each independent episode combines a manual procedure, where the SCS curve numbers are derived from field measurements

and normal antecedent moisture conditions (ACA, 2001), and an automatic procedure, using as an objective function the peak-weighted root mean square error and applying the univariate-gradient search algorithm method (USACE-HEC, 2000). The objective function, Z, is an index of goodness-of-fit to compare the computed and the observed hydrograph and it is defined as:

$$Z = \sqrt{\frac{1}{NQ}\Big[\sum_{i=1}^{NQ}\Big(q_o(i) - q_s(i)\Big)^2\Big(\frac{q_o(i) + q_o(mean)}{2q_o(mean)}\Big)\Big]}$$

where NQ is the number of computed hydrograph ordinates; $q_o(i)$ the observed flow at time i; $q_s(i)$ the simulated flow at time i, computed with a selected set of model parameters; and $q_o(mean)$ the mean of observed flows. Mathematically, it corresponds to searching for parameters that minimize the value of the objective function. The search is a trial-and-error search. Initial parameters are selected, the model is run and the errors are computed. If the error in not acceptable, HEC-HMS changes the initial parameters and reiterates. The decisions about these changes rely on the univariate gradient search algorithm.

The univariate-gradient search algorithm in HEC-HMS makes successive corrections to the parameter estimate. If x^k represents the parameter estimate with objective function $f(x^k)$ at iteration k, the search defines a new estimate x^{k+1} at iteration k+1 as

$$x^{k+1} = x^k + \Delta x^k \quad \text{where } \Delta x^k\text{=correction of the parameter}$$

The goal of the search is to select Δx^k so the estimates move toward the parameter that yields the minimum value of the objective function. If the correction does not reach the minimum value, this equation is applied recursively. The gradient method is based upon the Newton's method, which combined with the last equation derive to

$$\Delta x^k = -\frac{df(x^k)/dx}{d^2 f(x^k)/dx^2}$$

The process continues until additional adjustments will not decrease the objective function by at least 1%.

The curve number (CN) values derived from each of the five episodes are averaged per subbasin. In addition and following the same methodology, the flood wave celerity

for the main streams is also considered as a calibration index -by means of K parameter- owing to the nature of these kind of episodes characterized by very high flow velocities. With the intention of capturing as well as possible the flow wave celerities involved in the Montserrat extreme episode, the maximum propagation velocities obtained among the previous calibration episodes were used. The calibrated parameters were then used to run HEC-HMS for the 'Montserrat' case during a 96h simulation, from 9 June 2000 at 00:00 LT to 12 June 2000 at 24:00 LT, with a 10 minute time-step. This period completely encompasses the flood event and the subsequent hydrograph tail.

The previous calibration process and subsequent rain-gauge driven runoff simulations have been repeated for three spatial disaggregations of the catchment (21, 39 and 60 subbasins) with 1h accumulated rainfall discretization and varying temporal resolutions of the incoming rainfall data (30-min, 1-h and 3-h) with a 39 subbasins segmentation, in order to explore the sensitivities of the Llobregat basin and find an optimum configuration of the modelling system. The next section is fully devoted to this issue.

2.1.3 Sensitivity analysis to the spatial and temporal rainfall scales

In order to study the effects of the spatial scales of the rainfall field on the total basin response, the sensitivity of the catchment to three different spatial segmentations was evaluated: the basin was broken down into 21, 39 and 60 subbasins and the rainfall-runoff model was forced with hourly accumulated rainfall. The skill of the resulting runoff simulations is expressed in terms of the Nash-Sutcliffe efficiency criterion (NSE; Nash and Sutcliffe 1970), a 'goodness-of-fit' measure widely used in hydrological model validation (Jasper et al. 2003; Dolciné et al. 2001). The NSE values can range from $-\infty$ to 1, with higher values indicating a better agreement of the model results with the observations. NSE is defined as:

$$NSE = 1 - \frac{\sum_{i=1}^{n}(x_i - y_i)^2}{\sum_{i=1}^{n}(x_i - \overline{x})^2}$$

where x_i and y_i are the observed and model simulated discharged values at flow gauge site at time i, respectively, and $\overline{x}$ is the mean observed value. This same index will be

used in next sections to evaluate other spatial and temporal series.

The performance of the runoff simulations is also checked by means of the relative error of total volume at flow-gauge sites, expressed as percentage (%EV):

$$\%EV = (\frac{V_s - V_o}{V_o}) \cdot 100$$

where V_o and V_s are the observed and simulated runoff volumes, respectively. Therefore, %EV>0 and %EV<0 would indicate an over and underestimation of the volume by the model, respectively.

Table 2.2 shows the skill indices for the five calibration episodes. The results suggest a choice of 39 subbasins. For the Montserrat flash-flood (table 2.3) the optimum evaluation configuration in terms of model performance corresponds to 39 subbasins, particularly for the smallest watersheds, at Súria and Sant Sadurní gauges ($\sim$1000 km^2). For the largest basins, with areas exceeding 3000 km^2, the distinction is not so clear, and in Castellbell the 60 subbasins subdivision appears to be superior. The last two downstream gauges (Abrera and Castellbell) present similar statistical scores among the three discretizations, though the 39 subbasins configuracion is slightly superior (see fig. 2.8a for basin outlet). In general, then, the rainfall-runoff model reproduces better the 'Montserrat' event by dividing the Llobregat basin in 39 subbasins.

Flood events	***NSE 21-sb***	***%EV 21-sb***	***NSE 39-sb***	***%EV 39-sb***	***NSE 60-sb***	***%EV 60-sb***
16-19 Nov 1996	0.27	24.1	0.87	-1.3	0.83	-2.2
16-19 Dec 1997	0.25	57.5	0.84	21.3	0.31	54.0
17-20 Oct 2001	0.67	34.3	0.55	-10.3	0.62	-17.7
03-06 Dec 2003	0.46	30.9	0.77	25.1	0.90	-0.3
29-31 Aug 2004	0.27	27.9	0.43	17.6	0.40	46.2

Table 2.2: NSE efficiency criterion and percentage of error in volume (%EV) for the calibration episodes at the stream-gauges indicated in table 2.1. Three different basin configurations (21, 39 and 60 subbasins) and hourly accumulated rainfall are used.

	NSE 21-sb	***%EV 21-sb***	***NSE 39-sb***	***%EV 39-sb***	***NSE 60-sb***	***%EV 60-sb***
Súria	0.64	23.9	0.84	4.8	0.50	-33.7
Sadurní	0.46	11.6	0.67	12.4	0.50	-23.3
Castellbell	0.64	12.3	0.68	14.5	0.78	-5.4
Abrera	0.91	12.3	0.93	12.6	0.89	-2.1
Despí	0.82	3.6	0.84	1.1	0.76	8.4

Table 2.3: NSE efficiency criterion and percentage of error in volume (%EV) for the Montserrat evaluation event. The SAIH rain-gauge driven simulations are carried out with three different basin segmentations (21, 39 and 60 subbasins) at the five stream-gauges indicated. Hourly accumulated rainfall is used in all cases.

This result appears to be related to the number of rain-gauges lying inside the whole basin (36), implying an average area per station of 136.5 km^2. This area can be compared with the mean size of the 21, 39 and 60 subcatchments: 241.7 km^2, 126.0 km^2 and 81.9 km^2, respectively. Therefore, for 21 subbasins the model hyetograph tends to overlap information of several rain-gauges per subbasin, smoothing out detailed information of the spatial structure of the rainfall field that the rain-gauge network is able to resolve. On the contrary, for 60 subbasins the rainfall-runoff model does not acquire reliable information of the rainfall field for ungauged catchments. The configuration using 39 subbasins seems to optimize the performance of the simulated basin response, since it represents more adequately the truly resolved spatial variabilities of the rainfall field. It is worth noting that the differences in the outflow characteristics at the flow-gauges among the three watershed discretizations disminishes at larger scales (table 2.3).

In order to study the effects of the temporal scales of the rainfall field on the total basin response, the sensitivity of the catchment using a 39 subbasins segmentation together with 30 minutes, 1h and 3h accumulated rainfall discretizations have been analyzed for the calibration and Montserrat episodes (tables 2.4 and 2.5). Table 2.4 displays weak differences among the three temporal discretizations at the flow gauges indicated in table 2.1. The NSE and %EV skill scores results in table 2.5 indicate that the hourly discretization optimizes the simulation of the Llobregat basin response to the Montserrat

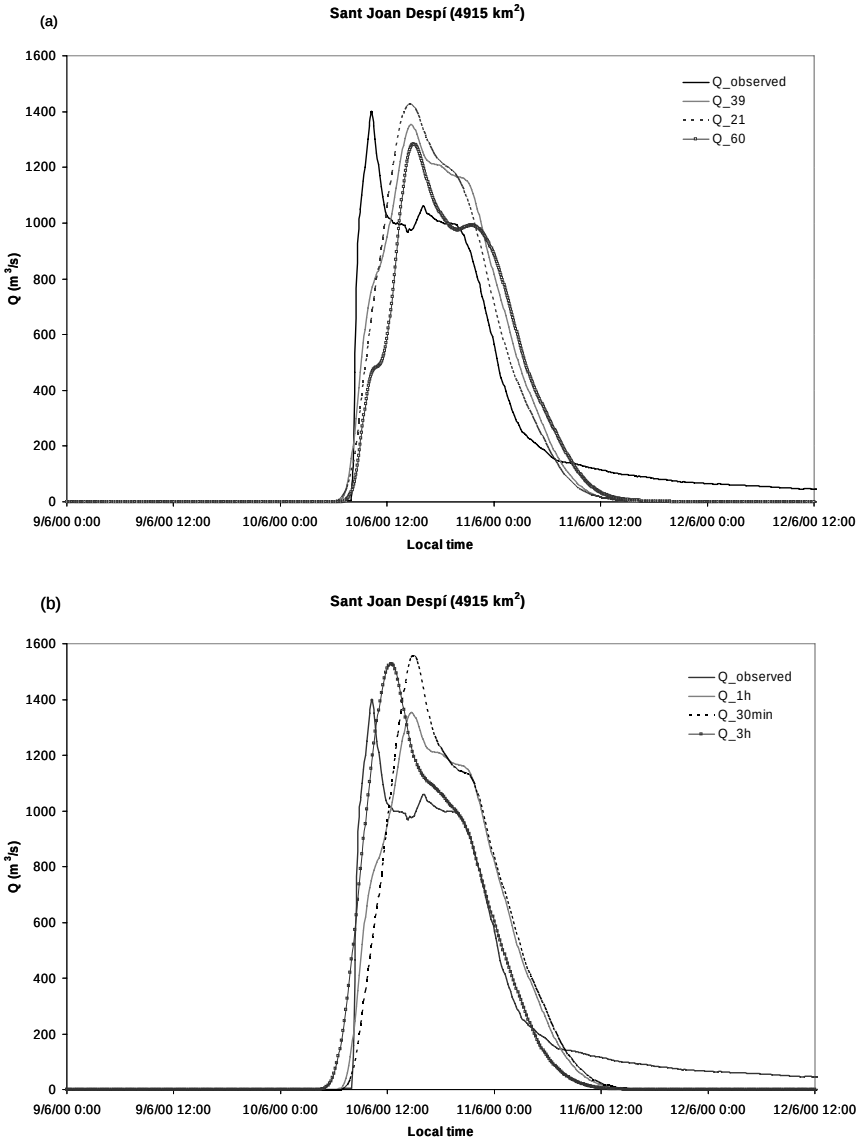

Figure 2.8: SAIH rain-gauge driven runoff discharge at Sant Joan Despí for the different (a) spatial and (b) temporal discretizations.

event, since it presents the best performance in three of the five flow sites and a notable reproduction of the observed flow at the remaining gauges. Nevertheless, slightly better accuracy at the basin outlet is exhibited by the 3h rainfall field discretization experiment (fig. 2.8b). With the exception of Sant Joan, the hydrographs computed at the different flow gauges (not depicted) show greater peak discharges for the 30 minutes evaluation experiment and faster response times for the 3h discretization when compared with observed. This result agrees with the notion that the higher the temporal variability of rainfall the greater the peak discharges, and also that a 3h temporal discretization may be inappropriate for strong storms and/or watersheds with fast response times (Singh 1997).

Flood events	*NSE 30-min*	*%EV 30-min*	*NSE 1-h*	*%EV 1-h*	*NSE 3-h*	*%EV 3-h*
16-19 Nov 1996	0.90	3.0	0.87	-1.3	0.89	3.3
16-19 Dec 1997	0.87	17.6	0.84	21.3	0.84	21.2
17-20 Oct 2001	0.70	-8.0	0.55	-10.3	0.70	-6.7
03-06 Dec 2003	0.88	10.7	0.77	25.1	0.89	14.2
29-31 Aug 2004	0.50	-0.1	0.43	17.6	0.50	-3.1

Table 2.4: NSE efficiency criterion and percentage of error in volume (%EV) for the calibration episodes at the stream-gauges indicated in table 2.1. Three different temporal discretizations (30-min, 1-h and 3-h) and 39 subbasins segmentation are used.

	NSE 30-min	*%EV 30-min*	*NSE 1-h*	*%EV 1-h*	*NSE 3-h*	*%EV 3-h*
Súria	0.91	-12.7	0.84	4.8	0.80	-9.9
Sadurní	0.58	23.5	0.67	12.4	0.64	12.3
Castellbell	0.62	18.5	0.68	14.5	0.39	16.0
Abrera	0.91	16.0	0.93	12.6	0.87	13.0
Despí	0.73	-0.5	0.84	1.1	0.90	2.4

Table 2.5: NSE efficiency criterion and percentage of error in volume (%EV) for the Montserrat evaluation event. The SAIH rain-gauge driven simulations are carried out with three different time-scale discretizations (30-min, 1-h and 3-h) at the five stream-gauges indicated. 39 subbasins segmentation is used in all cases.

From the set of the evaluation experiments analyzed, it seems that the most appropriate coherence between the spatial and temporal scales of the flash flood event that the raingauge network is able to resolve, is reached for 39 subbasins combined with 1h input rainfall data in the hydrological model (tables 2.3 and 2.5). This is the configuration of the model that will be used for the mesoscale model driven runoff simulations. Tables 2.6 and 2.7 report the main hydrological model parameters: curve numbers, initial abstractions, times of concentration and routing parameters.

subbasin	***CN***	I_a***(mm)***	***Tc(h)***	***subbasin***	***CN***	I_a***(mm)***	***Tc(h)***
1	71.6	21.5	3.1	21	60.7	41.1	3.0
2	75.5	23.0	1.4	22	60.4	43.0	2.6
3	78.3	20.8	1.3	23	63.4	29.7	3.0
4	69.0	29.6	2.8	24	63.1	51.0	2.2
5	72.1	22.4	2.0	25	66.1	46.2	3.0
6	59.5	64.5	1.6	26	61.8	42.0	1.8
7	58.8	38.0	2.0	27	67.1	31.0	1.6
8	64.5	34.1	2.3	28	69.4	33.6	2.0
9	62.6	59.9	1.7	29	63.6	45.6	2.2
10	63.4	50.4	2.0	30	63.6	35.5	1.6
11	52.8	43.6	1.6	31	68.1	37.8	2.0
12	69.1	19.6	1.1	32	60.3	79.7	0.6
13	71.0	26.0	1.5	33	56.7	76.2	1.9
14	71.6	32.2	1.8	34	63.5	62.8	1.6
15	70.9	27.9	1.6	35	54.0	77.1	2.2
16	67.0	28.4	1.7	36	56.1	61.1	2.2
17	68.6	33.0	2.2	37	56.8	74.4	1.6
18	62.1	37.1	2.1	38	59.1	85.1	2.0
19	67.5	26.1	1.0	39	55.6	77.4	2.1
20	62.7	28.9	2.4				

Table 2.6: Curve numbers, initial abstractions (in mm) and times of concentration (in h) for the selected basin configuration (displayed in Fig. 1.6).

reach	***K(h)***	χ	***reach***	***K(h)***	χ	***reach***	***K(h)***	χ
	Llobregat			Cardener			Anoia	
R1	1.4	0.20	R1	1.4	0.25	R1	1.6	0.20
R2	0.8	0.20	R2	0.6	0.30	R2	0.3	0.25
R3	0.3	0.20	R3	0.4	0.20	R3	1.4	0.25
R4	0.6	0.25	R4	2.0	0.25	R4	1.2	0.30
R5	1.2	0.25	R5	1.6	0.30	R5	1.0	0.35
R6	1.0	0.25	R6	1.0	0.35			
R7	1.0	0.25	R7	0.8	0.35			
R8	1.4	0.25	R8	3.0	0.35			
R9	1.4	0.25						
R10	3.1	0.25						
R11	3.0	0.25						
R12	3.2	0.30						
R13	2.7	0.30						

Table 2.7: Muskingum parameters for the selected basin configuration. Numeration of the river reaches follows the upstream direction (see Fig. 1.6).

2.2.1 A brief description of the mesoscale model

The non-hydrostatic MM5 numerical model is used to perform the meteorological simulations. It is a high resolution short-range weather forecast model developed by the Pennsylvania State University (PSU) and the National Center for Atmospheric Research (NCAR) (Dudhia 1993; Grell et al. 1995). The main characteristics of the model are briefly summarized:

(a) The MM5 model vertical and horizontal grids

The mesoscale model processes the data on pressure surfaces and this information has to be interpolated to the vertical coordinate of the MM5. The dimensionless vertical coordinate (σ) is defined as

$$\sigma = \frac{p - p_t}{p_s - p_t} \tag{2.1}$$

where p is the pressure, p_t is a constant top pressure, p_s is the surface pressure and each model level is defined by a value of σ ($0 \leq \sigma \leq 1$). This vertical coordinate is a terrain following variable: the lower grid levels follow the terrain while the upper surface is flat (fig. 2.9). Thus, the model vertical resolution is defined by a list of values between 0 and 1 not necessarily even spaced, and commonly, the resolution in the boundary layer is much finer than above.

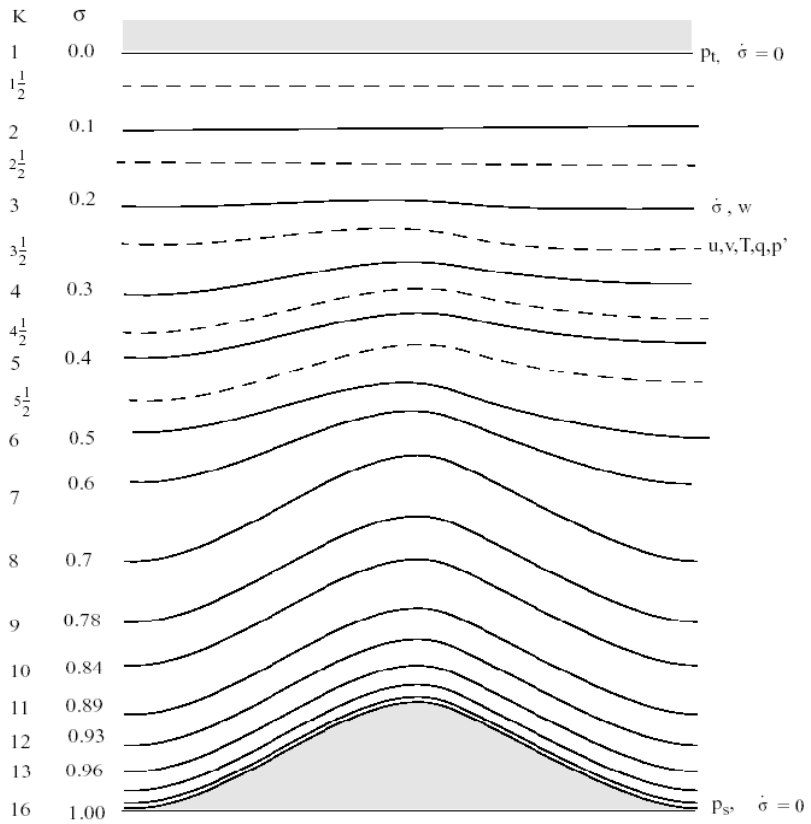

Figure 2.9: Schematic representation of the vertical structure of the model. The example is for 15 vertical layers. Dashed lines denote half-sigma levels, solid lines denote full-sigma levels.

The horizonal grid has an Arakawa-Lamb B-staggering of the velocity variables with respect to the scalars (fig. 2.10). Therefore, the scalars are defined at the center of the grid square, while the eastward (u) and northward (v) velocity components are located at the corners. All the variables are defined in the middle of each model vertical layer referred to as half-levels. Vertical velocity is carried at the full levels including levels at 0 and 1.

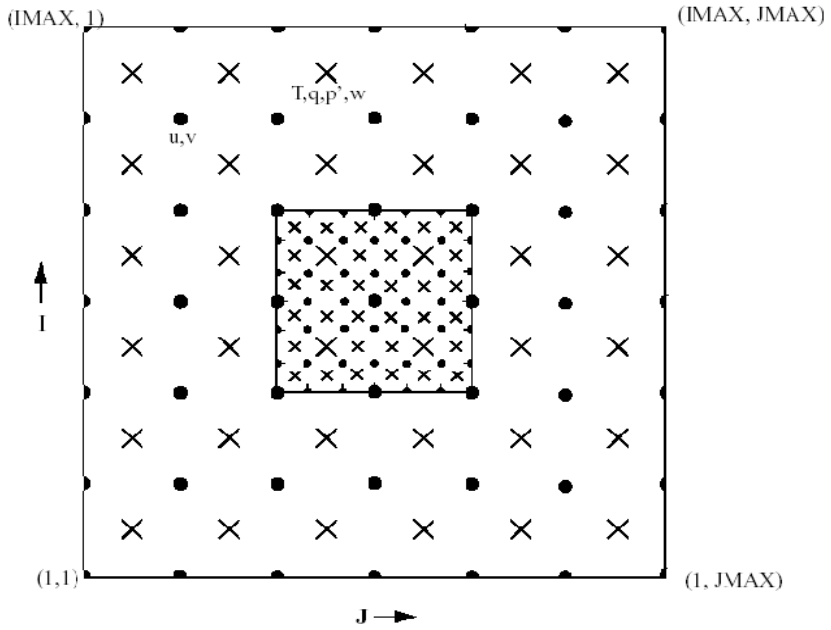

Figure 2.10: Schematic representation showing the horizontal Arakawa B-grid staggering of the dot and cross grid points. The smaller inner box is a representative mesh stagerring for a 3:1 coarse-grid distance to fine-grid distance ratio.

(b) The nesting capability

The MM5 model contains a capability of multiple nesting with several domains running at the same time and completely interacting (see fig. 2.11 as a possible configuration). Furthermore it permits a two-way interaction, thus the input data from a coarse to a fine domain come via its boundaries, while the feedback to the coarser mesh occurs over the interior nest. Each sub-domain has a 'mother domain' in which is completely embedded. There are three ways of doing a two-way nesting: (i) nest interpolation, where the nest is initialized by interpolating the coarse-mesh fields; (ii) nest analysis input, which permits the inclusion of high-resolution topography and initial analyses in the nest and (iii) nest terrain input, where the meteorological fields are interpolated from the coarse mesh and vertically adjusted to a new topography. It is also possible the one-way nesting in MM5. The model is run to create the output fields which are interpolated to the fine domain and an additional boundary field is also created once the one-way nested domain location

is specified. Therefore the one-way nesting differs from the two-way nesting in having no feedback and a coarser temporal resolution at the boundaries.

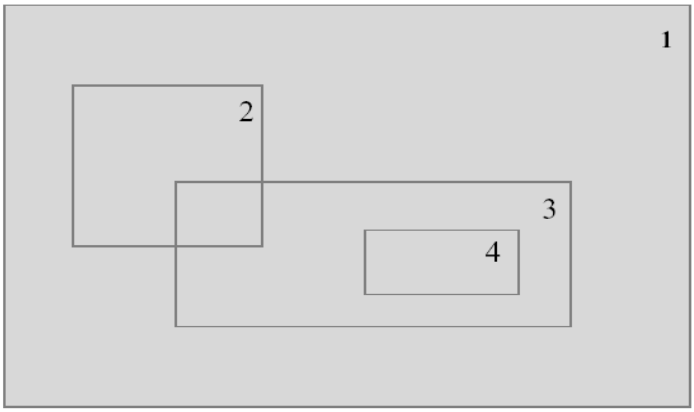

Figure 2.11: Example of a nesting configuration. The shading shows three different levels of nesting.

(c) The lateral boundary conditions

The regional numerical weather prediction models require lateral boundary conditions to run. In MM5 all lateral boundaries have specified horizontal winds, temperature, pressure and moisture fields and these can have specified microphysical fields (e.g clouds) whether are available. Before to running a simulation, the boundary conditions have to be set in addition to the initial values for these fields. The boundary values can come from Global Climate Models (GCMs) at different spatial and temporal resolutions. As an example, the NCEP and ECMWF centers issue these daily outputs at 1.125^0 - 0.5^0 and each 12 - 6 hours respectively and these can be used for weather prediction. Furthermore, the boundary and initial values can come from analyses which are generated from observations for a determined geographical region. The abovemetioned centers can also provide these analyses at different spatial and temporal resolutions. From the observations and by mean of various numerical interpolation methods it can be generated these tridimensional atmospheric fields in order to initialize the mesoscale model. The MM5 ingests these

discrete-time analyses by linearly interpolating them into its own time-step. Then, the analyses completely specify the behaviour of the lateral boundaries of the domain. Very close to the edge domain, the model is nudged towards the analyses and these are also smoothed, since the strength of this nudging decreases linearly away from the boundaries. The 2-way nest boundaries are similar but are updated every coarse-mesh time-step and have no relaxation zone.

(d) The nonhydrostatic dynamics

The mesoscale models are hydrostatic when the typical horizontal grid sizes are comparable with or greater than the vertical depth of features of interest. Then it is accomplished that

$$dp = -\rho_0 g dz \tag{2.2}$$

and when the hydrostatic approximation holds, the pressure is completely determined by the overlying mass of air. However, when the scale of resolved features in the model have aspect radios nearer unity, or when the horizontal scale becomes shorter than the vertical scale, nonhydrostatic dynamics must be considered.

The additional term in nonhydrostatic dynamics is the vertical acceleration that contributes to the vertical pressure gradient and the hydrostatic balance is no longer exact. Pressure perturbations from a reference state together with vertical momentum become extra three-dimensional predicted variables that have to be initialized.

(e) The reference state in the nonhydrostatic model

The reference state is an idealized temperature profile in hydrostatic equilibrium described by the equation:

$$T_0(p_0) = T_{s0} + A log_e(\frac{p_0}{p_{00}}) \tag{2.3}$$

where T_0 is specified by the sea-level pressure, p_{00}, taken to be 10^5 Pa, the reference temperature T_{s0} at p_{00} and a measure of lapse rate, A, equal to 50 K and representing the temperature difference between p_0 and $p_0/e = 36788Pa$. T_{s0} needs to be selected based on a typical sounding in the domain.

The surface reference pressure therefore depends entirely upon the terrain height. Using (2.2) and (2.3),

$$Z = -\frac{RA}{2g}(ln\frac{p_0}{p_{00}})^2 - \frac{RT_{s0}}{g}(ln\frac{p_0}{p_{00}}) \tag{2.4}$$

that can be solved for p_0 given Z, the terrain elevation. The heights of the model, the σ levels, are found from

$$p_0 = p_{s0}\sigma + p_{top} \quad \text{where} \tag{2.5}$$

$$p_{s0} = p_0(surface) - p_{top} \tag{2.6}$$

and this expression is used to find Z from p_0.

(f) The land-use categories

The MM5 model has the option of three sets of land-use categorizations. These have 13, 16 or 24 categories (e.g. type of vegetation, desert, urban, water, ice,...). To each grid cell of the model is assigned one of the categories, and this determines surface properties such as albedo, roughness length, longwave emissivity, heat capacity and moisture availability. The values are also variable according to summer or winter season.

(g) The basic equations of the MM5 model

The MM5 numerical model solves the following nonhydrostatic basic prognostic equations (moisture equation is omitted in this brief presentation). These are summarized in terms of terrain following coordinates (x, y, σ):

1. The pressure tendency equation

$$\frac{\partial p'}{\partial t} - \rho_0 g\omega + \gamma p \bigtriangledown \cdot \mathbf{V} = -\mathbf{V} \cdot \bigtriangledown p' + \frac{\gamma p}{T}(\frac{\dot{Q}}{c_p} + \frac{T_0 D_\theta}{\theta_0}) \tag{2.7}$$

where p' is the nonhydrostatic perturbation of the hydrostatic pressure, p; ρ_0 is the density of the air; $\gamma = c_p/c_v$ where c_p is the calorific heat of the air at constant pressure and, c_v, at constant volume; $\dot{Q}$ the heat exchange with the environment; T_0 the temperature of the buoyancy term; θ_0 the reference potential temperature and D_θ the heat loss owing to friction and turbulence. This equation relates the temporal

variations of the pressure with the rising and subsidence motions of the fluid, the pressure changes due to convergences or divergences, the pressure advection term and the variations of pressure by heat exchanges.

2. The three component momentum equations

$$\frac{\partial u}{\partial t}+\frac{m}{\rho}(\frac{\partial p'}{\partial x}-\frac{\sigma}{p^*}\frac{\partial p^*}{\partial x}\frac{\partial p'}{\partial \sigma})=-\mathbf{V}\cdot\bigtriangledown u+v(f+u\frac{\partial m}{\partial y}-v\frac{\partial m}{\partial x})-e\omega cos\alpha-\frac{u\omega}{r_{earth}}+D_u \tag{2.8}$$

where the terms are referred to: the map-scale factor (m); $p^*=p_{surf}-p_{top}$; the Coriolis force terms (f, $e=2\Omega cos\lambda$, $\alpha=\phi-\phi_c$ where λ is the latitude and ϕ, ϕ_c are the longitude and the central longitude); the curvature effect terms $(u\partial m/\partial y, v\partial m/\partial x, r_{earth})$; and D_u the heat losses term. The x-component momentum variations are related to the spatial variations of the pressure field, the advection of the x-component velocity, the effects owing to the curvature changes and the Coriolis force. The expressions for the y and z components follow as

$$\frac{\partial v}{\partial t}+\frac{m}{\rho}(\frac{\partial p'}{\partial y}-\frac{\sigma}{p^*}\frac{\partial p^*}{\partial y}\frac{\partial p'}{\partial \sigma})=-\mathbf{V}\cdot\bigtriangledown v-u(f+u\frac{\partial m}{\partial y}-v\frac{\partial m}{\partial x})+e\omega sin\alpha-\frac{v\omega}{r_{earth}}+D_v \tag{2.9}$$

$$\frac{\partial \omega}{\partial t}-\frac{\rho_0}{\rho}\frac{g}{p^*}\frac{\partial p'}{\partial \sigma}+\frac{g}{\gamma}\frac{p'}{p}=-\mathbf{V}\cdot\bigtriangledown\omega+g\frac{p_0}{p}\frac{T'}{T_0}-g\frac{R_d}{c_p}\frac{p'}{p}+e(ucos\alpha-vsin\alpha)+\frac{u^2+v^2}{r_{earth}}+D_\omega \tag{2.10}$$

where R_d is the universal constant of the dry air.

3. The thermodynamic equation

$$\frac{\partial T}{\partial t}=-\mathbf{V}\cdot\bigtriangledown T+\frac{1}{\rho c_p}(\frac{\partial p'}{\partial t}+\mathbf{V}\cdot\bigtriangledown p'-\rho_0 g\omega)+\frac{Q}{c_p}+\frac{T_0}{\theta_0}D_\theta \tag{2.11}$$

where the temperature rate change is related to the termic advection and the variations of the temperature owing to dinamical effects, heat exchanges and heat losses.

2.2.2 Application to the Montserrat flash-flood event

Simulations are designed using 24 vertical σ-levels and three spatial domains with 82×82 grid points (fig. 2.12). Their respective horizontal resolutions are 54, 18 and 6 km, with integration time-steps of 162, 54 and 18 seconds. The domains are centered in northeast Spain where the convective episode developed. In particular, the finest domain spans the entire Catalan territory and contiguous land and oceanic areas, and is used to supply the high-resolution rainfall fields to drive the hydrologic simulations. The interaction between the domains follows a two way nesting strategy (Zhang et al. 1986).

To initialize the model and to provide the time-dependent boundary conditions, NCEP and ECMWF meteorological grid analysis are used. MM5-NCEP simulation uses the analysis from the Global American Center for Enviromental Prediction for the large domain, and are updated every 12 hours with a 2.5^0 spatial resolution. MM5-ECMWF simulation uses the analysis of the European Center for Medium Range Weather Forecasts, with a spatial resolution of 0.3^0 and an update frequency of 6 hours. In both cases the first guess fields interpolated from the analyses on the MM5 model grid are improved using surface and upper-air observations with a successive-correction objective analysis technique (Benjamin and Seaman 1985). The tendencies along the model coarse domain boundaries, specified by differences of the fields between the 12h and 6h apart analyses, respectively, are applied using a Newtonian relaxation approach (Grell et al. 1995).

To parameterise moist convective effects the Betts-Miller cumulus scheme (Betts and Miller 1986) is used in the large domain and the Kain-Fritsch parametrization scheme (Kain 2002) in the intermediate domain. No convection scheme is in principle used in the inner one owing to the high horizontal resolution. Explicit microphysics is represented in all domains with prediction equations for cloud and rain water fields, cloud ice and snow allowing for slow melting of snow, supercooled water, graupel and ice number concentration (Reisner et al. 1998). The planetary boundary layer physics is formulated using a modified version of the Hong and Pan scheme (Hong and Pan 1996). Surface temperature over land is calculated using a force-restore slab model (Blackadar 1979; Zhang and

Anthes 1982) and over sea it remains constant during the simulations. Finally, long and short wave radiative processes are formulated using the RRTM scheme (Mlawer et al. 1997).

Furthermore, since it is debatable whether a 6 km resolution domain can resolve convection appropriately without a convection scheme, an additional experiment has been designed. This simulation, labeled as MM5-NCEP-4D, coincides with MM5-NCEP except that it applies the Kain-Frist scheme for the third domain. It also incorporates a fourth domain of 2 km horizontal resolution forced in two way mode, in which convection is fully explicit. The possible benefits of enhanced horizontal resolution in this complex orographic region can thus be assessed.

With the purpose of generating the ensemble of perturbed simulations, the invertibility principle of Ertel potential vorticity (PV)(Hoskins et al. 1985) is applied . In particular, we are interested in studying the sensitivity of the Montserrat hydro-meteorological event to uncertainties in the precise representation of the upper-level precursor trough (shown in fig. 2.12), being aware that small scale aspects of the circulation are propitious to analysis or forecast errors. The piecewise PV inversion scheme described in Davis and Emanuel (1991) is then used as a clean approach to manipulate the upper-level synoptic trough in the model initial conditions. What it is necessary is a simple identification of the PV signature of the trough (shown as shaded in fig. 2.12) and then the balanced mass and wind fields associated with that PV element can be used to alter the meteorological fields in a physically consistent way (effectively, a change in the structure or position of the trough). This method has already shown its value for assessing the predictability of flash flood events in the western Mediterranean area (e.g. Romero 2001; Homar et al. 2002; Romero et al. 2005).

Using the NCEP-derived initial conditions, the upper-level trough intensity is perturbed $\pm 5\%$ (simulations -5% PV and +5% PV) and its position is displaced ± 54 km along the zonal direction (experiments WEST and EAST). This short ensemble of simulations is a first approximation to the problem of incorporating the spatio-temporal uncertainty of the rainfall forecast into a medium size catchment like the Llobregat basin.

The whole set of MM5 simulations comprises a 36 hour period, from 9 June 2000 at 00:00 UTC to 10 June 2000 at 12:00 UTC, after the end of the rainfall event in Catalonia.

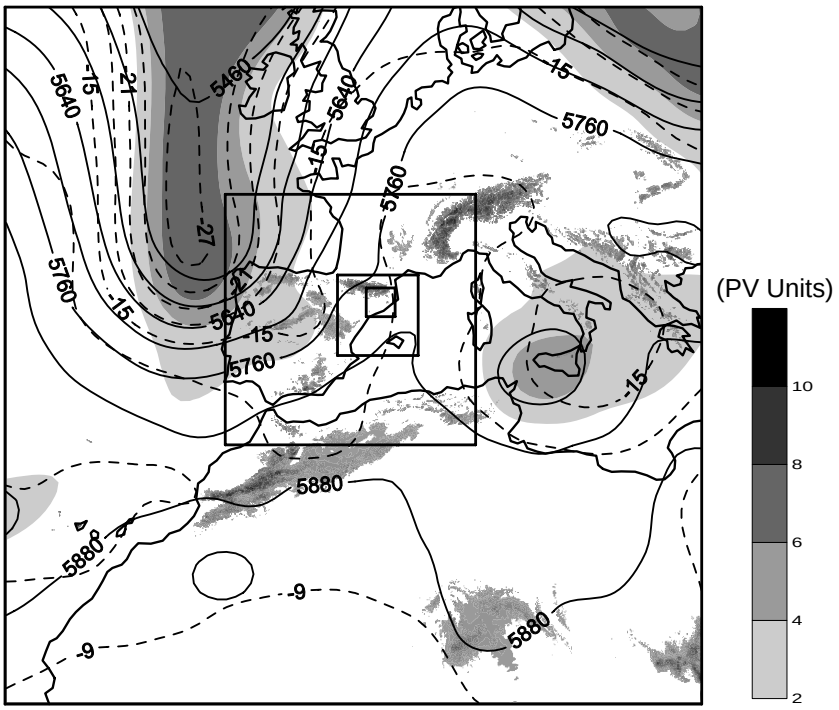

Figure 2.12: Configuration of the four computational domains used for the MM5 numerical simulations (horizontal resolutions are 54, 18, 6 and 2 km, respectively) and MM5-NCEP simulation initial state, showing geopotential height at 500 hPa (continuous line, in gpm), temperature at 500 hPa (dashed line, in ${}^0C$) and isentropic PV on the 330 K surface (shaded, according to scale) at 00 UTC 9 June 2000.

Chapter 3

RESULTS AND DISCUSSION

3.1 SAIH rain-gauge driven runoff simulation

SAIH rain-gauge derived rainfall of the 'Montserrat event' is used to drive the calibrated HEC-HMS model in a single evaluation runoff simulation according to the methodology described in chapter 2. Figure 3.1a displays the spatial distribution of the accumulated rainfall upon the entire watershed and figures 3.2 and 3.3 show, respectively, the accumulated volume per subbasin and the temporal sequence of accumulated volume over the entire basin at hourly time-steps. These distributions will be compared against the simulated ones in next sections.

As a general overview, table 3.1 and figure 1.9 show a good HEC-HMS skill for the characterization of the Llobregat basin response to the 'Montserrat' event. NSE exceeds 0.65 in the set of flow-gauges, and particularly at Abrera it exceeds 0.9. Relative errors in volume are reasonably small and only at Castellbell the error is close to 15%, though in all the stream-gauges the volume is overestimated. Therefore, the results indicate a reasonable goodness-of-fit for the main peak discharges, their timing and the volume estimations at the flow-gauges. For small-scale features, however, the rain-gauge driven run shows some inaccuracies: at Súria, multiple peaks are simulated instead of a single one (fig. 1.9a); at Sadurní, Castellbell and Abrera, the opposite case occurs and the model only simulates an envelope of the higher frequency peaks (fig. 1.9b, c and d); at Sant Joan Despí, a significant delay occurs in the time to peak (fig. 1.9e).

	NSE SAIH	***%EV SAIH***	***NSE NCEP***	***%EV NCEP***	***NSE NCEP-4D***	***%EV NCEP-4D***
Súria	0.84	4.8	0.60	-16.9	0.67	-2.3
Sadurní	0.67	12.4	-0.12	-100	-0.12	-100
Castellbell	0.68	14.5	0.19	35.5	0.47	-49.2
Abrera	0.93	12.6	0.58	15.9	0.36	-55.8
Despí	0.84	1.1	0.51	-12.0	0.21	-66.8

Table 3.1: NSE efficiency criterion and percentage of error in volume (%EV) at the five stream-gauges for the SAIH rain-gauge driven and MM5-NCEP driven runoff simulations with three (NCEP) and four domains (NCEP-4D).

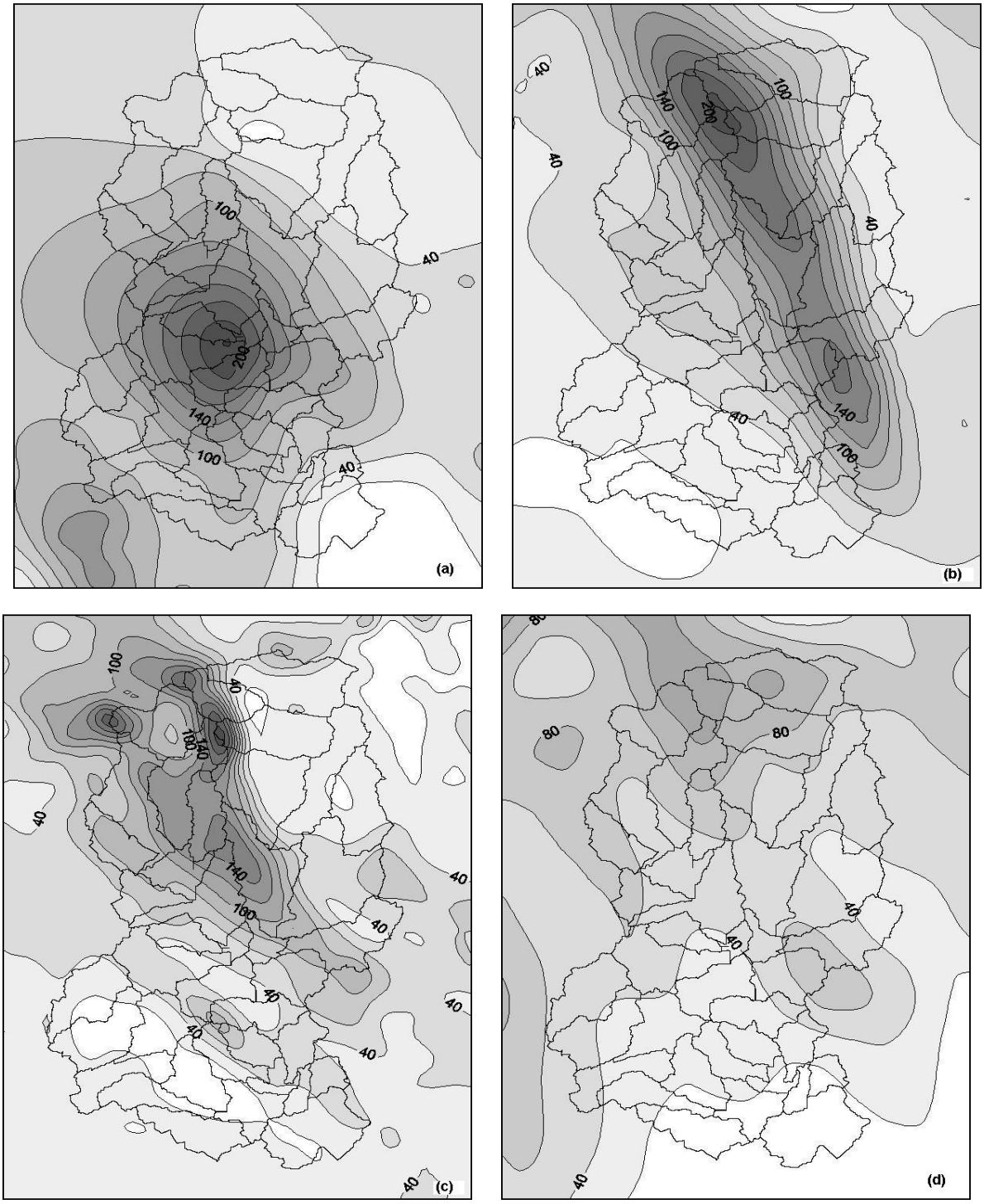

Figure 3.1: Spatial distribution of accumulated rainfall during the 'Montserrat' eventin the Llobregat basin, from: (a) SAIH rain-gauges, (b) MM5-NCEP simulation, (c) MM5-NCEP-4D simulation and (d)MM5-ECMWF simulation . Contour interval is 20 mm starting at 20 mm.

3.2 MM5-NCEP, MM5-NCEP-4D and MM5-ECMWF driven runoff simulations

To assess the skill of the MM5 mesoscale runs, the spatial and temporal distributions of the simulated rainfall volume are compared against the rain-gauge derived volume pattern. The spatial comparison is done using the 39 subbasins as accumulation units for the whole episode, and the temporal comparison uses hourly accumulations for the whole basin. The degree of agreement between model and observed rainfall distributions is quantified using the NSE and root mean square error (RMSE) statistical indices (table 3.2). With regard to the spatial distribution, the best skill scores are obtained by the MM5-ECMWF and MM5-NCEP-4D experiments. The MM5-NCEP experiment shows a moderately worse behaviour, but on the contrary, it is the best for the temporal distribution.

	NSE spatial	***NSE temporal***	***RMSE spatial***	***RMSE temporal***
NCEP	-1.52	0.74	9.3	11.2
NCEP-4D	-0.36	0.64	6.8	13.2
ECMWF	-0.62	0.51	7.5	15.4
-5%PV	0.39	0.66	4.6	12.7
+5%PV	-2.05	0.56	10.3	14.6
WEST	-0.47	0.39	7.1	17.1
EAST	-2.59	0.56	11.1	14.5

Table 3.2: NSE efficiency criterion and root mean square error (RMSE, in hm^3) of the spatial and temporal rainfall volume distributions yielded by the set of mesoscale numerical simulations.

From a hydrological point of view, the MM5-NCEP simulation is the most suitable, attending to total precipitated water over the Llobregat basin, discharged volume at the basin outlet (table 3.3), and the amount of the maximum hourly precipitated volume in the basin (table 3.4).

	Precipitated volume	***Discharged volume***
SAIH	405.7	72.4
NCEP	378.5	64.5
NCEP-4D	307.0	24.4
ECMWF	252.3	10.1
-5%PV	394.1	75.3
+5%PV	253.8	30.8
WEST	355.7	60.1
EAST	301.2	50.6

Table 3.3: Total precipitated volume (hm^3) in Llobregat basin, and discharged volume (hm^3) at Sant Joan Despí outlet, from SAIH rain-gauges and the set of mesoscale numerical simulations. Observed discharged volume by the SAIH stream-gauge was 73.2 hm^3.

	Maximum volume	***Local time***
SAIH	72.0	06:00
NCEP	71.3	07:00
NCEP-4D	46.9	07:00
ECMWF	53.1	08:00
-5%PV	67.5	08:00
+5%PV	53.8	06:00
WEST	78.5	08:00
EAST	61.5	04:00

Table 3.4: Maximum 1h accumulated volume for the whole Llobregat basin (hm^3) and its corresponding local time (on 10 June, 2000), from SAIH rain-gauges and the set of mesoscale numerical simulations.

The superior behaviour in these aspects of the MM5-NCEP rainfall simulation can be appreciated in figures 1.9, 3.2 and 3.3 and table 3.1. MM5-ECMWF driven runoff simulation is not shown owing to its low skill on reproducing the episode, with corresponding statistical scores at the Llobregat basin outlet of NSE=-0.19 and %EV=-86.3. Figure 3.1d reveals that the MM5-ECMWF rainfall field is very deficient for this particular case study (compare with fig. 3.1a). In addition, the MM5-NCEP-4D driven runoff simulation exhibits a remarkable underestimation of the peak discharges and volumes at the different stream-gauges, except at Súria (fig. 1.9 and table 3.1). The MM5-NCEP-4D rainfall field contains very fine spatial features owing to the inclusion of the 2 km resolution forcing in the simulation (fig. 3.1c), but the quantitative and spatial rainfall forecast is not better than the MM5-NCEP result (fig. 3.1b). The inclusion of a convective scheme in the third domain appears to have a negative impact on the simulation. Therefore, MM5-NCEP simulation is chosen as the *c*ontrol simulation for this investigation.

The most remarkable deficiency of the control simulation is the north-eastward shift of the rainfall pattern towards higher terrain and a more elongated shape with regard to the observed distribution, although with similar amounts (fig. 3.1). It seems reasonable to argue that the catchment's complex orography, dominated by the Pyrenees, the pre-coastal and coastal ranges is a determinant factor for the mesoscale model to produce that spatial distribution. Nevertheless, the simulated heavy rainfall lies within the Llobregat basin and the simulated timing of the rainfall episode is remarkably good (fig. 3.3), in benefit of the MM5-NCEP driven runoff simulation. Since the MM5 control simulation tends to concentrate the maximum rainfall towards the upper part of the basin, where the two reservoirs are located, then it would be expected a significant effect of hydrograph diffusion in the runoff. For the reservoir located in the Llobregat river, with an initial volume of 95 hm^3 and an inflow volume of 14.0 hm^3, the resulting outflow volume is 12.2 hm^3. The peak discharge disminishes from 560.8 $m^3\ s^{-1}$ to 145.4 $m^3\ s^{-1}$ with an attending delay close to 8 hours. The diffusion effect by the reservoir located in the Cardener river is smaller: a decrease from 96.6 $m^3\ s^{-1}$ to 71.6 $m^3\ s^{-1}$ with a delay of about 1.5 hours.

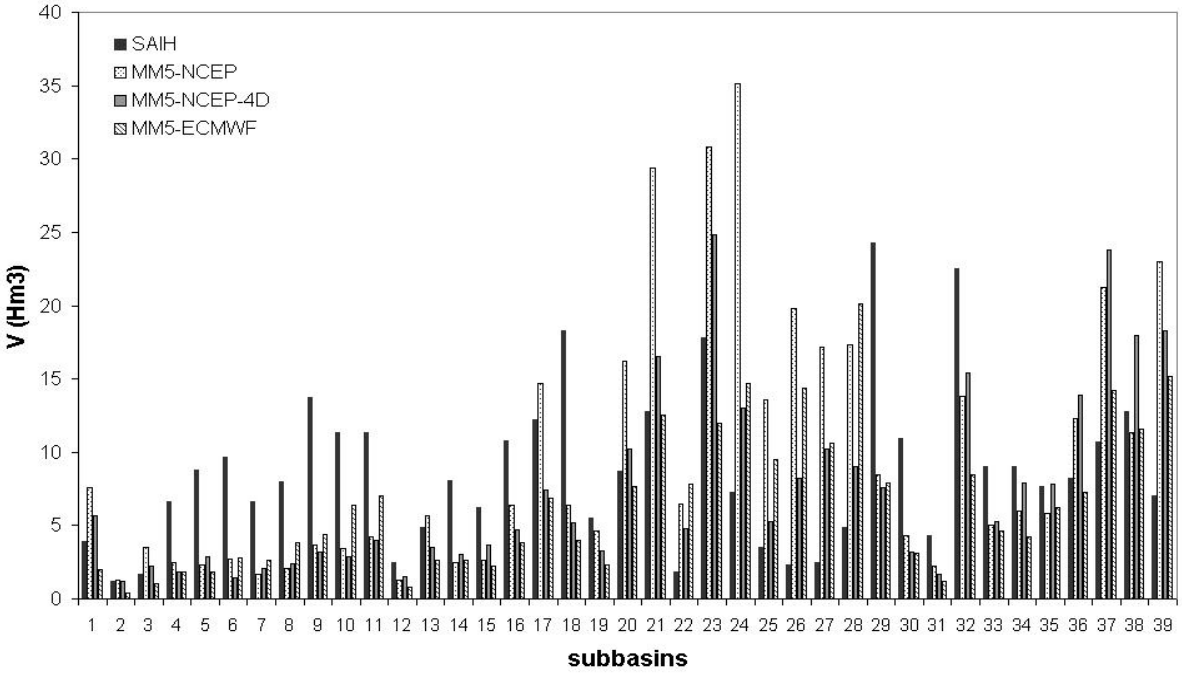

Figure 3.2: Accumulated volume during the 'Montserrat' event, per subcatchment of the Llobregat basin, from SAIH rain-gauge, MM5-NCEP, MM5-NCEP-4D and MM5-ECMWF simulations. See Fig. 1.6 for subcatchment numbering.

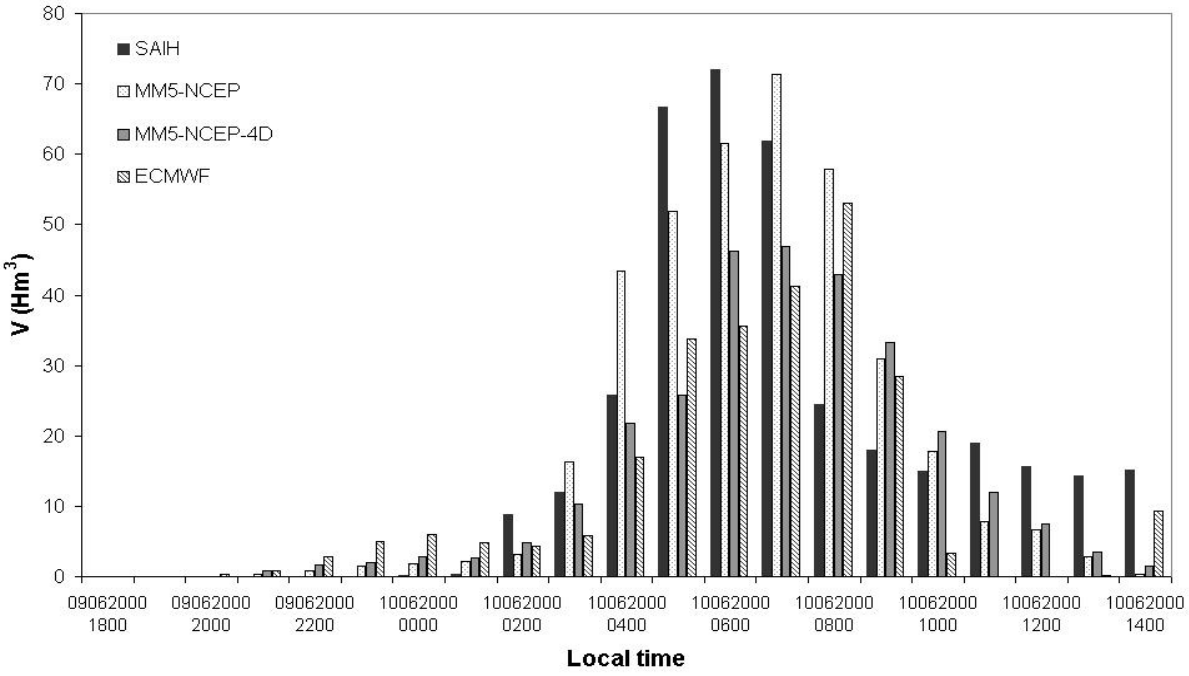

Figure 3.3: Temporal sequence, at 1h time steps, of accumulated volume in the Llobregat basin during the 'Montserrat' event, from SAIH rain-gauge, MM5-NCEP, MM5-NCEP-4D and MM5-ECMWF simulations.

The MM5-NCEP driven runoff simulation at Súria site displays a good agreement with the observed peak discharge but not with its timing (fig. 1.9a; table 3.1). At Sant Sadurní site the simulation is very deficient and no runoff is produced (fig. 1.9b; table 3.1): the mesoscale model widely underestimates the rainfall amounts in the Anoia watershed (compare figs. 3.1a and 3.1b and see fig. 3.2). At Castellbell and Abrera sites, runoff is widely overestimated producing a large error in the peak estimation and, consequently, making these results less suitable for use in emergency management directives (figs. 1.9c and d). As the hydrograph is routed downstream, the overestimation of the runoff volume decreases owing to the deficit of the simulated rainfall in the southwestern subbasins which contribute to the inflow. Another characteristic feature of the simulated runoff hydrographs along the Cardener and Llobregat rivers is a lag-time of around 3 hours with respect to the observed flows, which is consistently routed downstream towards the basin outlet (fig. 1.9e). This is due to several factors: the aforementioned hydrograph

diffusion by the basin's reservoirs, the fact that the core of the simulated heavy rainfall occurs further upstream and with a certain delay compared with the observations, and the exceptional flood wave propagation for this particular event.

3.3 Ensemble of MM5-perturbed driven runoff simulations

Following the PV inversion method described in section 2.2, four additional mesoscale runs (-5% PV, +5% PV, WEST and EAST) are performed in order to produce MM5-perturbed driven runoff simulations. These simulations, together with the previously referenced experiments MM5-NCEP, MM5-NCEP-4D and MM5-ECMWF, become a useful experimental dataset to investigate the effects of the uncertainty of the mesoscale model initial conditions on the hydrometeorological chain. It is well-known (e.g. Ferraris et al. 2002) that even slight spatial and temporal errors of the rainfall pattern can have a significant impact on the response of small catchments (up to hundreds of km^2). However, the spatio-temporal gap between operational meteorological model outputs, and the required hydrological model inputs, should be considerably smoothed for a basin of medium size (thousands of km^2). The results in the last section showed that the Llobregat basin was reasonably capable of filtering the forecast rainfall errors as long as the main rainfall nuclei lie within the catchment (tables 3.1 and 3.2). Our hypothesis is that the basin should be relatively insensitive to realistic perturbations of the rainfall field introduced through the PV inversion method, and therefore the predictability of flash flood events should be appreciable in this medium size catchment. The use of ensemble strategies like the one tested here should provide a very useful probabilistic approach to the problem in the context of real-time operations.

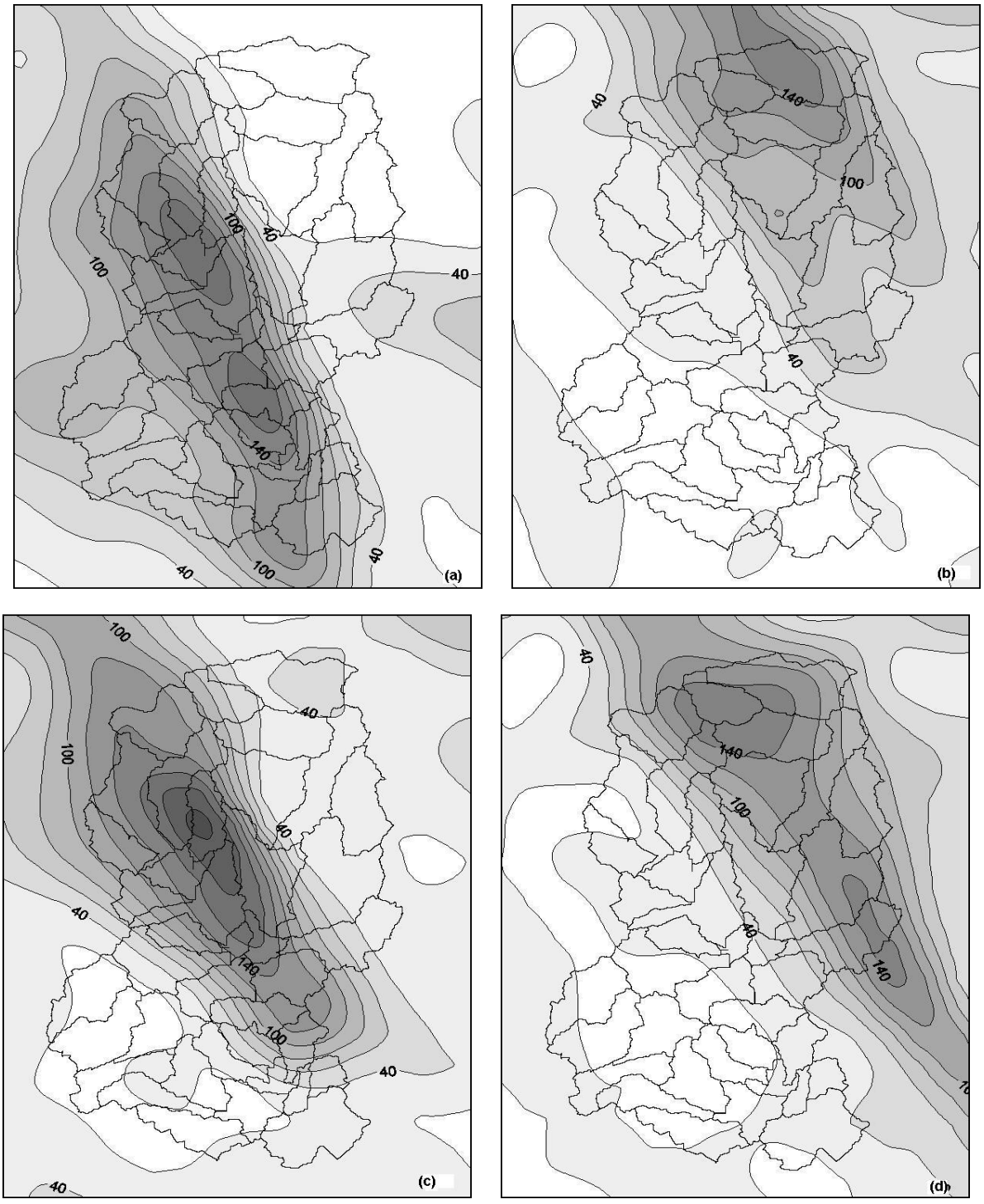

Figure 3.4: Spatial distribution of accumulated rainfall during the 'Montserrat' event in the Llobregat basin, from: (a) -5% PV, (b) +5% PV, (c) WEST, and (d) EAST simulations. Contour interval is 20 mm starting at 20 mm.

Figures 3.4 and 3.5 display the spatial distributions of accumulated rainfall volume for the perturbed experiments. The -5% PV and WEST simulations (figs. 3.4a and c) are fairly similar to the observed rainfall pattern (fig. 3.1a), such that the spatial goodness-of-fit statistical indices of forecast rainfall outperform the results of the reference MM5-NCEP simulation. On the contrary, the spatial errors of +5% PV and EAST simulations are greater than in the reference experiment (table 3.2). It seems, then, that a weaker or more distant upper-level precursor trough benefits the rainfall forecast of the Montserrat event. Pressumably, the resulting slower-moving surface cyclone is more representative of the actual disturbance.

Furthermore, the whole ensemble of perturbed experiments slightly underestimates the total water collected over the Llobregat basin as it occurred with MM5-NCEP, although the -5% PV slightly improves the control simulation, with only 11.6 hm^3 below the observed value (table 3.3). The underestimation of precipitated volume is particularly severe in the Anoia subcatchment, where only the -5% PV run is able to produce appreciable values of rainfall (fig. 3.4). Even so, the runoff simulation at Sant Sadurní gauge is rather poor, albeit for the rest of the ensemble dataset, runoff is not produced at all (table 3.5). In addition, tables 3.2 and 3.4 and figure 3.6 exhibit a certain uniformity in the temporal distributions of the rainfall volume for the perturbed experiments. Nevertheless, none of these prove to be superior in the temporal evolution to the control simulation. It is interesting to note that the ensemble of simulated rainfall fields exhibits a larger heterogenity in space than in time (compare the respective NSE indices; table 3.2).

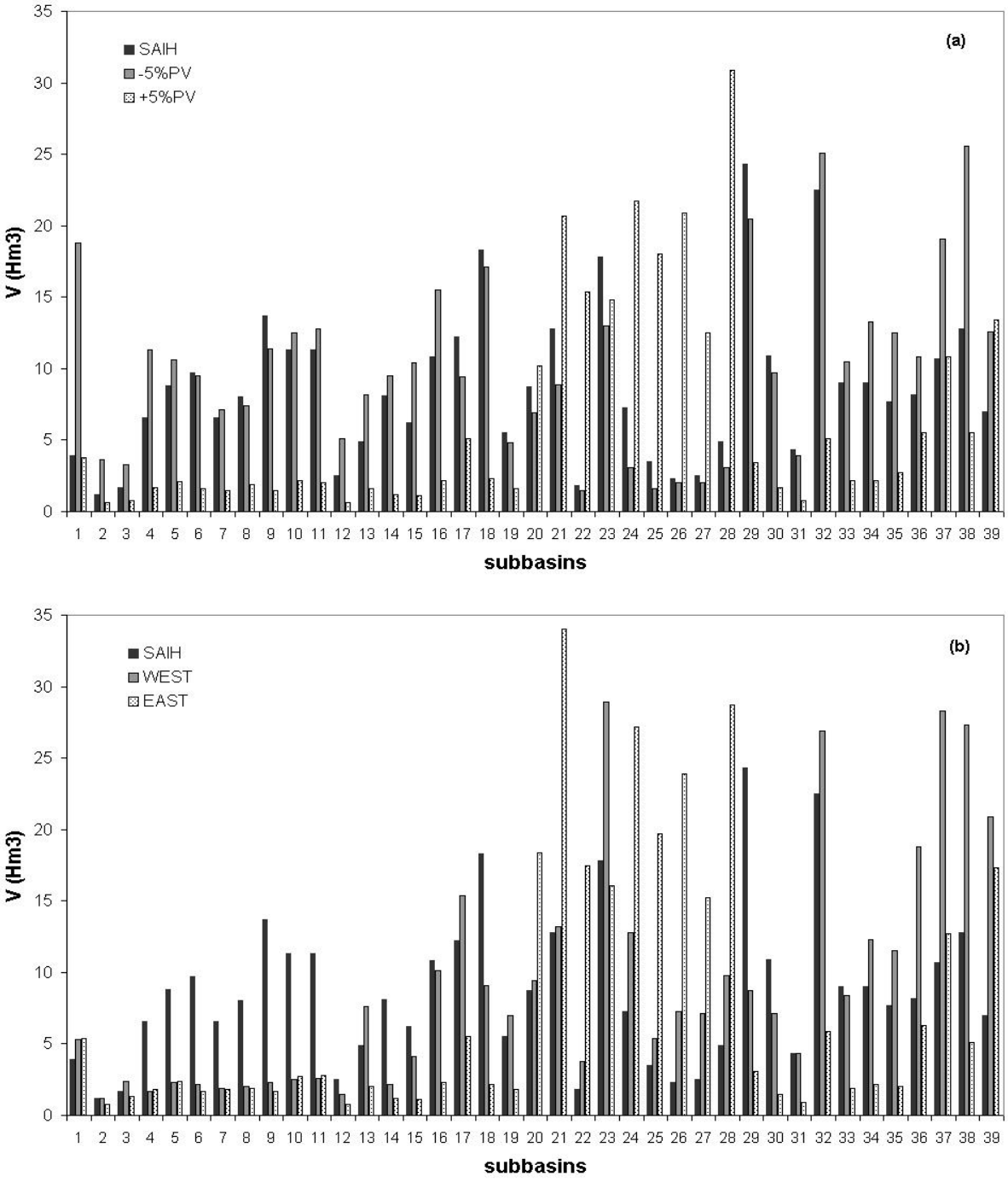

Figure 3.5: Accumulated volume during the 'Montserrat' event, per subcatchment of the Llobregat basin, from: (a) SAIH rain-gauges, -5% PV, and +5% PV simulations, and (b) SAIH rain-gauges, WEST, and EAST simulations.

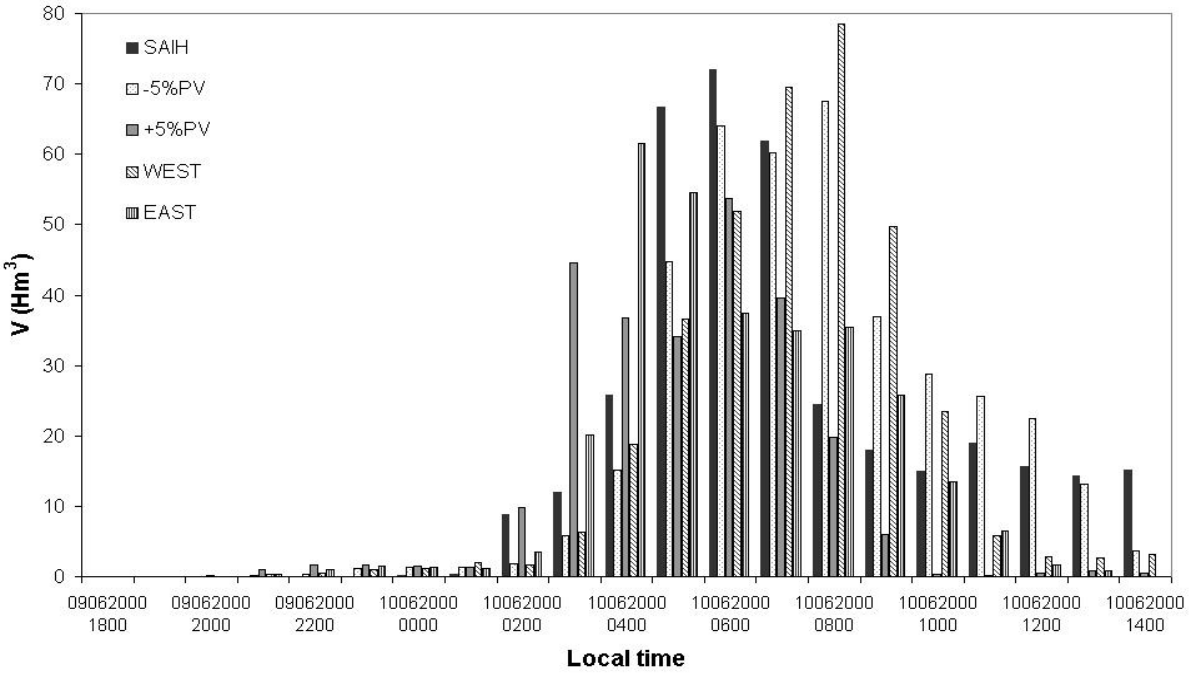

Figure 3.6: Temporal sequence, at 1h time steps, of accumulated volume in the Llobregat basin during the 'Montserrat' event, from: SAIH rain-gauges, -5% PV, +5% PV, WEST and EAST simulations.

Finally, table 3.5 summarizes the statistical indices at the five stream-gauges for the ensemble of perturbed runoff simulations. At small basin scales, the skill is rather low owing to the lack of coherence among the meteorological and hydrological spatio-temporal scales (figures not shown). But at larger scales, the skill of the ensemble to forecast the discharge is considerably improved (figs. 3.7a, b and c), to the extent that different members of the ensemble outperform the control simulation at different stream-gauges (e.g. Castellbell and Abrera). These results demonstrate the value of an ensemble strategy in order to obtain a higher confidence interval in mesoscale model driven rainfall-runoff forecasts and to enact the appropriate emergency directives.

		-5%PV	+5%PV	WEST	EAST
Súria	***NSE***	-0.62	-0.25	-7.97	-0.18
	% EV	75.6	-97.5	191.3	-86.4
Sadurní	***NSE***	-0.17	-0.12	-0.12	-0.12
	% EV	-33.9	-100	-100	-100
Castellbell	***NSE***	0.71	0.48	0.21	0.56
	% EV	-19.5	-31.0	20.1	12.8
Abrera	***NSE***	0.93	0.28	0.72	0.51
	% EV	-5.1	-41.8	7.6	-4.7
Despí	***NSE***	0.53	0.13	0.56	0.34
	% EV	2.8	-58.1	-17.9	-31.1

Table 3.5: NSE efficiency criterion and percentage of error in volume (% EV) at the five stream-gauges, for the set of MM5-perturbed driven runoff simulations.

Essentially, the full set of driven runoff simulations does not exhibit any strong degradation of the forecast skill, not accounting for the ECMWF analysis driven simulation. It appears, then, that this catchment as a whole is relatively insensitive to typical errors of the forecast rainfall, like spatial shifts of a few tenths of kilometers and temporal shifts of not more than 1-2 hours. The relative insensitivity of the Llobregat basin is surely a consequence of its medium size, and it is only lost for the smallest subbasins or when the heavy rainfall affects external hydrographic areas as for the ECMWF experiment. The filtering behaviour of rainfall uncertainty found for the Llobregat basin in this case could also be raised by the moderate urbanization density and the relatively high predictability of the responsible mesoscale convective system. For smaller basins intercepting significant urban areas or with very local thunderstorms the capability of filtering the rainfall uncertainty is generally not found (Gómez et al. 1998).

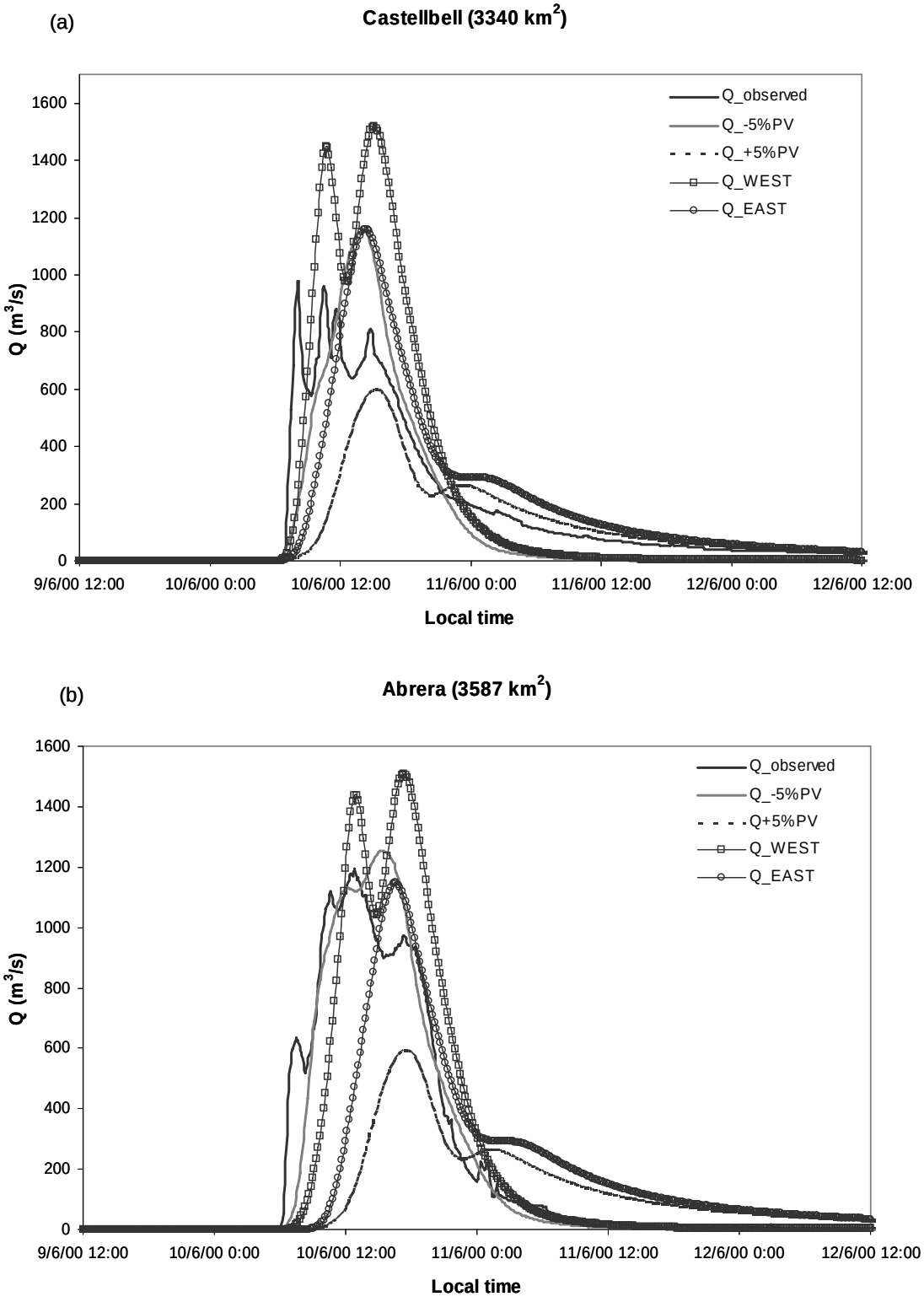

Figure 3.7: Observed, -5% PV simulation driven, +5% PV simulation driven, WEST simulation driven and EAST simulation driven runoff discharge at: (a) Castellbell, (b) Abrera and (c) Sant Joan Despí.

(c)

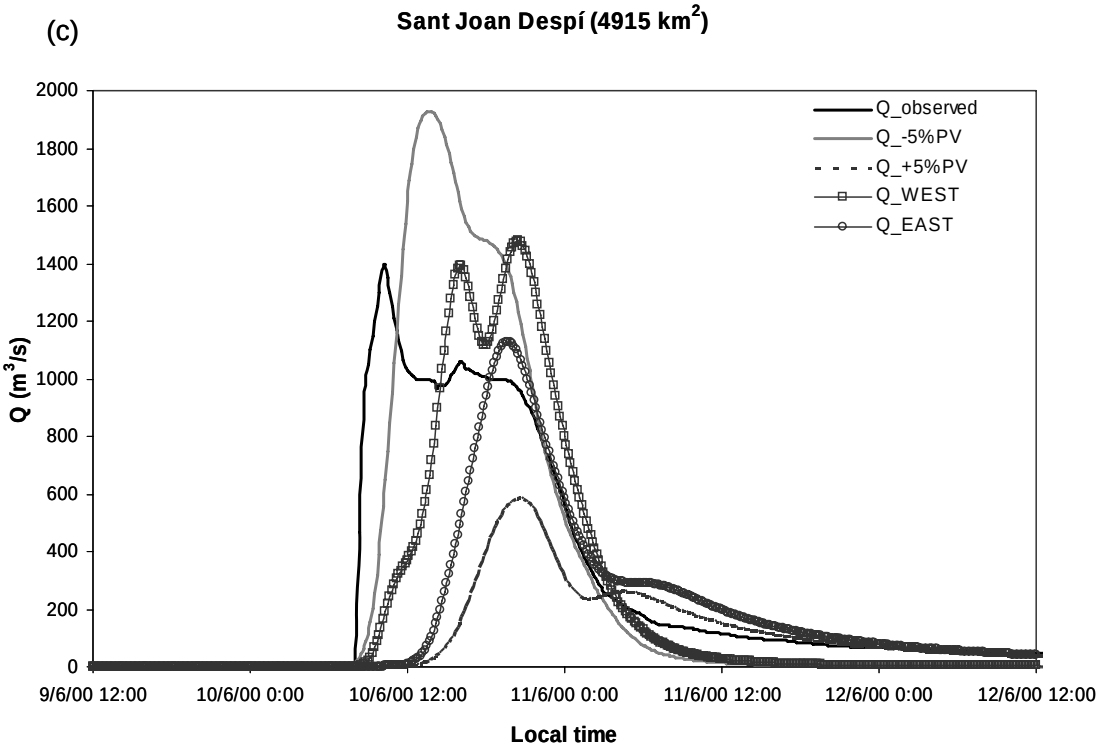
Sant Joan Despí (4915 km2)
Q_observed
Q_-5%PV
Q_+5%PV
Q_WEST
Q_EAST
Q (m3/s)
2000
1800
1600
1400
1200
1000
800
600
400
200
0
9/6/00 12:00
10/6/00 0:00
10/6/00 12:00
11/6/00 0:00
11/6/00 12:00
12/6/00 0:00
12/6/00 12:00
Local time

Chapter 4

CONCLUSIONS AND FURTHER REMARKS

This work has analysed the feasibility of runoff simulations driven by numerical weather prediction mesoscale models over the Llobregat basin, characteristic of the Spanish Mediterranean environment, in an attempt to understand the sensitivity of the basin response to forecast errors, and help to gain additional lead-times for warning and emergency procedures before flash flood situations. The effects of different spatial and temporal rainfall field scales on the basin response has been studied by breaking down the basin in three different segmentations and by considering three temporal scales in a set of six experiments. A configuration considering 39 subbasins division together with hourly temporal rainfall field discretization optimizes the basin response for the 'Montserrat' event. It appears that this result is particularly related to the current density of rain gauges available within or very near the catchment. Similar tests and a re-calibration of the runoff model should be applied using a long sample of mesoscale rainfall forecasts rather than rain-gauge information in order to properly optimize the numerical system for operational purposes, but this task is beyond the objectives and capabilities of the present study.

Hazardous events present short recurrence periods in Mediterranean Spain as a whole, and the 'Montserrat' event analysed in this study is a forceful proof of their possible consequences. Using NCEP and ECMWF analyses to initialize the hydro-meteorological chain, it was possible to obtain, at least at the basin outlet, reasonable runoff forecasts

with up to 12-48 hours lead-times in the first case. These control runs were complemented by an ensemble of driven rainfall-runoff simulations which showed to be useful to derive conclusions in depth. With the ensemble of MM5-NCEP perturbed simulations, it was possible to reduce the biases at some sites, as Castellbell and Abrera, where the control simulation would have not produced enough accurate runoff forecasts.

The set of perturbed mesoscale simulations was also introduced to address the effects of the meteorological external scale uncertainty. This source of uncertainty was reflected on the spatial and temporal distribution of the rainfall pattern in the Llobregat basin, with shifts of tenths of kilometers in the position of the heavy rainfall cores and changes of about 1-2 hours in their timing, in some cases outperforming the control run. Interestingly, the basin rainfall-runoff mechanisms were shown to smooth to a high degree the above spatial and temporal differences, thus enhancing, at least for this case, the predictability of flash floods in the Llobregat basin considering the entire catchment and the typical magnitude of mesoscale rainfall output errors. Nevertheless, one of the simulations of the ensemble -the MM5-ECMWF run- exhibited very poor results, and used in a deterministic hydro-meteorological system, would have missed completely the hazardous event and inhibit any standard emergency procedure. This is a good example where a simple multi-analysis ensemble prediction system (EPS) accounting for the forecast variance associated to the initial conditions uncertainty would have been found of great value to trigger special flood warnings. However, to further extend the derived results, rainfall forecast errors found in existing mesoscale models should be examined for their typical magnitude and variability in space and time. Obviously, the higher performance of the NCEP-based simulations is simply a particularity of the 'Montserrat' meteorological situation, and not an inherent aspect of this analysis dataset. It is reasonable to expect that the high resolution of ECMWF analyses would generally benefit nested mesoscale numerical forecasts in the region.

The methodology presented in this paper can be automated to obtain short-range runoff forecasts driven by high-resolution mesoscale predictions currently available in real-time (see for example http://mm5forecasts.uib.es). We believe that the enhanced

predictability shown here in the Llobregat basin as a whole would also apply to many other hazardous episodes, as well as to other Mediterranean catchments of similar size and physical characteristics. In addition, it must be noted that runoff predictions for use in emergency management directives may not need to match exactly the peak discharges or their timing. These predictions must simply reach suitable thresholds so as to cause the appropriate directives to be enacted (Anderson et al. 2002).

The precise hydrological response of a catchment to rainfall events, in terms of the induced runoff, is strongly determined by the spatial and temporal variability of the soil properties. The infiltration mechanism acts as a highly non linear filter in the rainfall-runoff transformation and it has been modeled as an integrated process over each subbasin at discrete time-steps. The model parameters related with this mechanism and with the flood wave routing have been calibrated using five events. These events are characterized by important discharges and high velocities of the associated flood waves, but the lack of flow data at some flow-gauges for some of these events has posed difficulties in the basin calibration. In order to improve the reliability and skill of the rainfall-runoff model before such hazardous episodes, it would be desirable to get more information of other flash-flood events affecting the Llobregat basin. The expected future increase of the number of recorded cases in the SAIH database, and a larger number of stream-gauges operating in the basin, will then permit an improvement of the basin configuration and the forecast and alert schemes.

In general, the set of driven rainfall-runoff simulations showed the lowest skill at the gauges covering small scales of the basin. None of the members of the ensemble, for example, was able to adequately reproduce the flow of the Anoia river for this episode, as an illustration of the forecasting limitations arisen as the hydrological scales of interest are decreased. Numerous techniques exist that attempt to mitigate this lack of coherence between the spatio-temporal scales of meteorological and hydrological models, particularly different applications of statistical downscaling (e.g. Clark and Hay 2004; Hewitson and Crane 1992; von Storch and Zwiers 1999; Wilks 1999; Antolik 2000) or disaggregation techniques (Deidda et al. 1999; Deidda 2000; Ferraris et al. 2002). These research lines

appear as of the maximum interest for future studies in order to develop the most suitable hydro-meteorological chain forecasting system upon the Spanish Mediterranean area.

REFERENCES

Agència Catalana de l'Aigua, 2001: *Delimiting of flood plain for the draft of the INUNCAT. Internal Basins of Catalonia. Hydrological calculations and determination of the flood wave discharge. Vol. 2.* Departament de Medi Ambient. Generalitat de Catalunya, 88 pp. (in catalan, available at: http://mediambient.gencat.net/aca/documents/ca/ planificacio /inuncat/conquesinternes/calculhidro_vii.pdf)

Agència Catalana de l'Aigua, 2003: *Technical recommendations for flood studies at local area.* Departament de Medi Ambient. Generalitat de Catalunya, 106 pp. (in catalan, available at: http://mediambient.gencat.net/aca/documents/ca/planificacio/criteris_tecnics/recomanacions_tecniques_estudis_inundabilitat.pdf)

Alpert, P., T. Ben-gai, A. Baharad, Y. Benjamini, D. Yekutieli, M. Colacino, L. Diodato, C. Ramis, V. Homar, R. Romero, S. Michaelides and A. Manes, 2002: The paradoxial increase of Mediterranean extreme daily data in spite of decrease in total values. *Geophys. Res. Lett.*, **20**, 1-4.

Anderson, M.L., Z.Q. Chen, M.L. Kavvas and A. Feldman, 2002: Coupling HEC-HMS with atmospheric models for prediction of watershed runoff. *J. Hydrol. Eng.*, **7**, 312-318.

Antolik, M.S., 2000: An overview of the National Weather Service's centralized statistical quantitative precipitation forecast. *J. Hydrol.*, **239**, 306-337.

Bacchi, B., A. Buzzi, G. Grossi and R. Ranzi, 2002: Flood forecasting in a midsize catchment in the southern Alps: Recent experiences on the use of couple meteorological and hydrological model. *Proceedings of the third EGS Plinius conference*, Baja Sardinia. Consiglio Nazionale delle Ricerche, Roma, Italy, 201-208.

Bellon, A. and I. Zawadzki, 1994: Forecasting of hourly accumulations of precipitation by optimal extrapolation of radar maps. *J. Hydrol.*, **157**, 211-233.

Betts, A.K. and M.J. Miller, 1986: A new convective adjustment scheme. Part II: single column using GATE wave, BOMEX, ATEX and Artic air-mass data sets. *Quart. J. Roy. Meteor. Soc.*, **112**, 693-709 pp.

Benjamin, S.G. and N.L. Seaman, 1985: A simple scheme for improved objective analysis in curved flow. *Mon. Wea. Rev.*, **113**, 1184-1198.

Blackadar, A.K., 1979: High resolution models of the planetary boundary layer. *Adv. Environ. Sci. and Eng.*, **1**, 50-85.

Brémaud, P.J. and Y. Pointin, 1993: Forecasting heavy rainfall from rain cell motion using radar data. *J. Hydrol.*, **142**, 373-389.

Castelli, F., 1995: Atmosphere modelling and hydrology prediction uncertainty. *Proc. U.S.-Italy Research Workshop on Hydrometeorology: Impacts and Management of Extreme floods*, Perugia, Italy, Water Resources Research and Documentation Center and Colorado State University, 13-17.

Chappell, C.F., 1986: Quasi-stationary convective events. *Mesoscale Meteorology and Forecasting*, P. S. Ray, Ed., Amer. Meteor. Soc., 289-298.

Chow, V.T., D.R. Maidment and L.W. Mays, 1988: *Applied hydrology.* McGraw-Hill International Editions. Civil engineering series. 572 pp.

Clark, M.P. and L.E. Hay, 2004: Use of medium-range numerical weather prediction model output to produce forecasts of stream-flow. *J. Hydrometeor.*, **5**, 243-262.

Conway, B.J. and K.A. Browning, 1988: Weather forecasting by interactive analysis of radar and satellite imagery. *Phil. Trans. Roy. Soc.*, **324**, 299-315.

Davis, C.A. and K.A. Emanuel, 1991: Potential vorticity diagnosis of ciclogenesis. *Mon. Wea. Rev.*, **119**, 1929-1953.

Deidda, R., R. Benzi and F. Siccardi, 1999: Multifractal modelling of anomalous scaling laws in rainfall. *Water Resour. Res.*, **35**, 1853-1867.

Deidda, R., 2000: Rainfall downscaling in a space-time multifractal framework. *Water Resour. Res.*, **36**, 1779-1794.

Dolciné, L., H. Andrieu, D. Sempere-Torres and D. Creutin, 2001: Flash flood forecasting with coupled precipitation model in mountainous mediterranean basin. *J. Hydrol. Eng.*, **6**, 1-9.

Doswell, C.A. 1994: Flash flood-producing convective storms: current understanding and rsearch. *Proceedings from Spain-U.S. joint workshop on natural hazards* Barcelona, Spain, 8-11 June 1993.

Doswell, C.A., H.E. Brooks and R. A. Maddox 1996: Flash flood forecasting: an ingredients-based methodology. *Wea. Forecasting.*, **11**, 560-581.

Dudhia, J., 1993: A nonhydrostatic version of the Penn State/NCAR mesoscale model: Validation tests and simulation of an Atlantic cyclone and cold front. *Mon. Wea. Rev.*, **121**, 1493-1513.

Ferraris, L., R. Rudari and F. Siccardi, 2002: The uncertainty in the prediction of flash floods in the Northern Mediterranean environment. *J. Hydrometeor.*, **3**, 714-727.

Gómez, M. and R. López, 1998: *Rehabilitation of sewer networks in member states. Sant Boi sewer network.* Research Report, European project SPRINT SP-98. (available at: Library of Universitat Politècnica de Catalunya, Barcelona, Spain)

Grell, G.A., J. Dudhia and D.R. Stauffer, 1995: *A description of the fifth-generation of the Penn State/NCAR mesoscale model (MM5)*, NCAR Tech. Note NCAR/TN-398+STR, Boulder, USA.

Groisman, P.Y., R.T. Karl, D.R. Easterling, R.W. Knight, P.F. Jamason, K.J. Hennessy, R. Suppiah, C.M. Page, J. Wibig, K. Fortuniak, V.N. Razukaev, A. Douglas, E. Førland and P.M. Zhai, 1999: Changes in the probability of heavy precipitation: important indicators od climatic change. *Clim. Chan.*, **42**, 243-283.

Hardaker, P.J., C.G. Collier and C.E. Pierce, 1994: The Gandolf system: A look to the future for operational flood forecasting using satellite and radar measurements. *Proc. British Hydrological Soc. Radar Meeting*, 39-63.

Hewitson, B.C. and R.G. Crane, 1992: Large-scale atmospheric controls on local precipitation in tropical Mexico. *Geophys. Res. Lett.*, **19**, 1835-1838.

Homar, V., R. Romero, C. Ramis and S. Alonso, 2002: Numerical study of the October 2000 torrential precipitation event over eastern Spain: Analysis of the synoptic-scale stationarity. *Ann. Geophys.*, **20**, 2047-2066.

Hong, S.-Y. and H.-L. Pan, 1996: Nonlocal boundary layer vertical diffusion in a medium-range forecast model. *Mon. Wea. Rev.*, **124**, 2322-2339.

Hoskins, B.J., M.E. McIntyre and A.W. Robertson, 1985: On the use and significance of isoentropic potential vorticity maps. *Quart. J. Roy. Meteor. Soc.*, **111**, 877-946.

Jasper, K. and P. Kaufmann, 2003: Coupled runoff simulations as validation tools for atmospheric models at the regional scale. *Quart. J. Roy. Meteor. Soc.*, **129**, 673-692.

Kain, J.S., 2004: The Kain-Fritsch convective parameterization: an update. *J. Appl. Meteor.*, **43**, 170-181.

Llasat, M.C., T. Rigo and M. Barriendos, 2003: The 'Montserrat-2000' flash flood event: a comparasion with the floods that have ocurred in the northeast iberian peninsula since the 14th century. *Int. J. Climat.*, **23**, 453-469.

Martín, A., R. Romero, V. Homar, A. de Luque, S. Alonso, T. Rigo and M.C. Llasat, 2006: Sensitivities of a flash-flood event over Catalonia: A numerical analysis. *Mon. Wea. Rev.* (in press).

Martín-Vide, J.P., D. Niñerola, A. Bateman, A. Navarro and E. Velasco, 1999: Runoff and sediment transport in a torrential ephemeral stream of the Mediterranean coast. *J. Hydrol.*, **225**, 118-129.

Menéndez, M., 1998: *Design discharge calculations and flood plain management.* CEDEX, Madrid. Research Report, European project Flood Aware: prevention and forecast of floods. (available at: http://www.lyon.cemagref.fr/projects/floodaware/ report/03cedex.pdf)

Mlawer, E.J., S.J. Taubman, P.D. Brown, M.J. Iacono and S.A. Clough, 1997: Radiative transfer for inhomogeneous atmosphere: RRTM, a validate correlated-k model for the long wave. *J. Geophys. Rev.*, **102** (D14), 16663-16682.

Murphy, A.H., 1993: What is a good forecast? An essay on the nature of goodness in Weather Forecasting. *Wea. Forecast.*, **8**, 281-293.

Nash, J.E. and J.V. Sutcliffe, 1970: River flow forecasting through conceptual models. Part I: A discussion of principles. *J. Hydrol.*, **10** (3), pp 282-290.

Orlanski, I. 1975: A rational subdivision of scales for atmospheric processes. *Bull. Amer. Meteor. Soc.*, **56**, pp 527-530.

Ramis, C., S. Alonso and M.C. Llasat, 1994: A comparative study between two cases of extreme rainfall events in Catalunya. *in Hydrometeorological Hazards in a Changing Perspective, Surveys in Geophysics*, **33**, 750.

Ranzi, R., B. Bacchi and G. Grossi, 2003: Runoff measurements and hydrological modelling for the estimation of rainfall volumes in an Alpine Basin. *Quart. J. Roy.*

Meteor. Soc., **129**, 653-672.

Reisner, J., R.J. Rasmussen and R.T. Bruintjes and G., 1998: Explicit forecasting of supercooled liquid water in winter storms using the MM5 mesoscale model. *Quart. J. Roy. Meteor. Soc.*, **124**B, 1071-1107.

Romero, R., C. Ramis, S. Alonso, C.A. Doswell III and D.J. Stensrud 1998: Mesoscale model simulations of three heavy precipitation events in the western Mediterranean region. *Mon. Wea. Rev.*, **126**, 1859-1881.

Romero, R., 2001: Sensitivity of a heavy rain producing Western Mediterranean cyclone to embedded potential vorticity anomalies.*Quart. J. Roy. Meteor. Soc.*, **127**, 2559-2597.

Romero, R., A. Martín, V. Homar, S. Alonso and C. Ramis, 2006: Predictability of prototype flash flood events in the western Mediterranean under uncertainties of the precursor upper-level disturbance. *Adv. Geosciencies*, **7**, 55-63.

Siccardi, F., 1996: Rainstorm hazards and related disasters in the western Mediterranean region. *Rem. Sens. Rev.*, **14**, 5-21.

Singh, V.P., 1997: Effect of spatial and temporal variability in rainfall and watershed characteristics on stream flow hydrograph. *Hyd. Proc.*, **11**, 1649-1669.

Témez, J.R., 1978: Cálculo hidrometeorológico de caudales máximos en pequeñas cuencas naturales. *MOPU*. Madrid.

US Army Corps of Engineers Hydrologic Engineering Center, 1998: HEC-HMS Hydrologic Modeling system user's manual, USACE-HEC, Davis, California. 188 pp. (available at: http://www.hec.usace.army.mil)

US Army Corps of Engineers Hydrologic Engineering Center, 2000: Hydrologic Mod-

eling system HEC-HMS. Technical reference manual. USACE-HEC, Davis, California. 157 pp. (available at: http://www.hec.usace.army.mil)

US Department of Agriculture, 1986: Urban hydrology for small watersheds. Technical release 55 of the Nature Resources Conservation Service. US Department of Agriculture. Washington DC, USA.

von Storch, H. and F.W. Zwiers, 1999: *Statistical Analysis in Climate Research.* Cambridge University Press, 494 pp.

Wilks, D., 1999: Multisite downscaling of daily rainfall with a stochastic weather generator. *Clim. Res.*, **11**, 125-136.

Zhang, D.L. and R.A. Anthes, 1982: A high resolution model of the planetary boundary layer. Sensitivity tests and comparisons with SESAME-79 data. *J. App. Meteor.*, **21**, 1594-1609.

Zhang, D.L. and J.M. Fritsch, 1986: Numerical simulation of the meso-β scale structure and evolution of the 1977 Johnstown flood. Part I: Model description and verification. *J. App. Meteor.*, **43**, 1913-1943.